University of Copenhagen

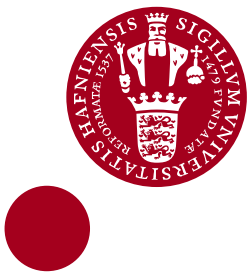

# An improved Gas-CFA system for methane measurements and preliminary results from the Dye-3 ice core

Janani Venkatesh

MSc Climate Change

Master Thesis (30 ECTS)

wjz988

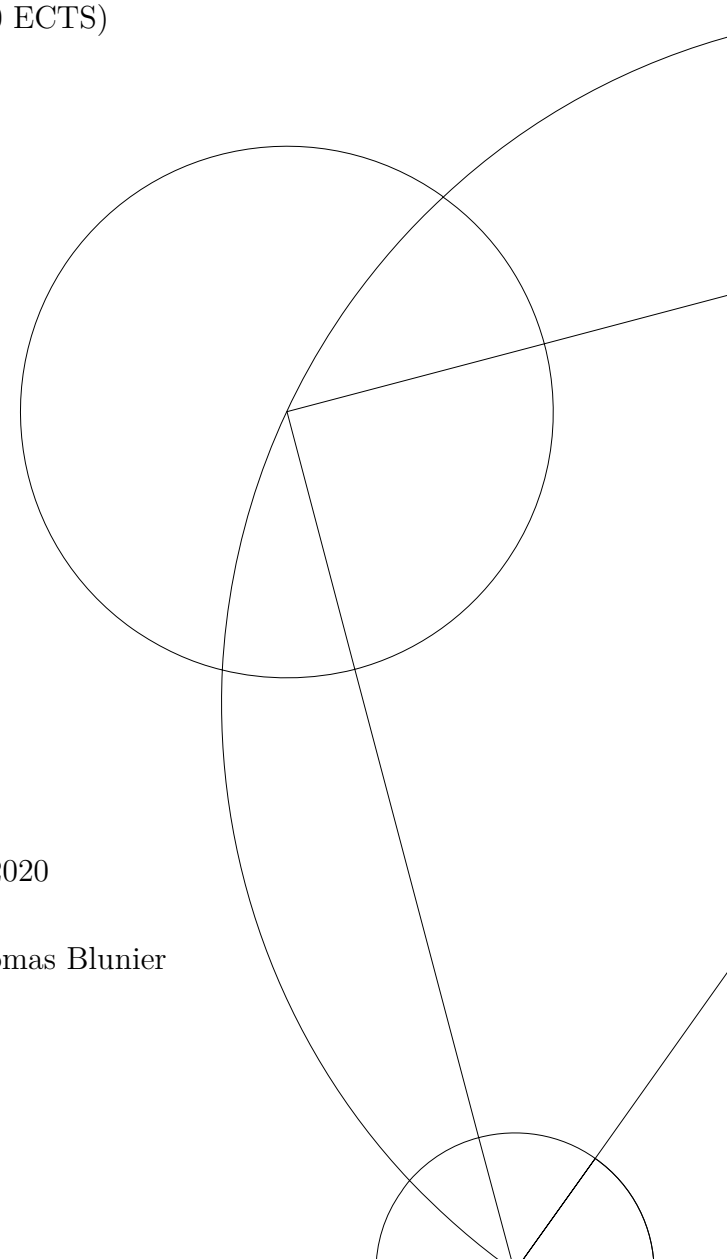

January 22, 2020

Supervisor: Prof. Thomas Blunier

**Abstract**

Gases in ice cores present the unique opportunity for studying the concentration of greenhouse gases during various climatic conditions of the past. The development of laser spectroscopy and Continuous Flow Analysis (CFA) techniques has introduced the possibility of high resolution gas measurements in ice cores. This report focuses on improving established techniques by addressing some of the uncertainties observed in previous gas-CFA set-ups. A hydrophobic membrane micromodule (MicroModule 0.75" X 1", 3M Liqui-Cel) has been used to replace the debubbler as the main gas extraction unit. A Wavelength-Scanned Cavity Ring-Down Spectrometer (WS-CRDS) (Picarro G-1101i trace gas analyzer, Picarro Inc.), operating at a cavity pressure of 45 Torr, is used to measure methane mixing ratios in the sample stream. The low cavity pressure of the WS-CRDS, along with a back pressure regulator, regulates the pressure gradient between the gas and liquid phase at the micromodule to ca. 700 mbar, facilitating high extraction efficiency. This system has been implemented in the Dye-3 CFA campaign in fall 2019, and the Younger Dryas section of the record is presented here to exemplify data corrections and quality. The uncertainty of measurements is estimated to be ca. $\pm 5$ ppbv, with a depth resolution of 4-8 cm of ice, depending on total gas content in the sample, leading to an estimated age resolution on a decadal scale for the Younger Dryas section. However, systematic offsets have been observed in the dataset compared to discrete measurements from other ice cores. These offsets lie beyond the range of measurement uncertainty and require further investigation. Furthermore, suggestions have been made based on the current work for future points of investigation, and potential upgrades to the system to improve data quality.

# Contents

## List of Abbreviations

The following is a list of abbreviations used and what they stand for, in alphabetical order

$Ar$ Argon

$B-A$ Bølling-Allerød

$BPR$ Back Pressure Regulator

$BPV$ Bypass Gas Standard Ball Valve

$CFA$ Continuous Flow Analysis

$CH_4$ Methane

$E_{eff}$ Extraction Efficiency

$FI_g$ Gas flow meter

$FI_{l_d}$ Liquid flow meter - Dust

$FI_l$ Liquid flow meter - Module

$GISP2$ Greenland Ice Sheet Project 2

$GRIP$ Greenland Ice Core Project

$GWP$ Global Warming Potential

$H_2O$ Water

$HPFA$ High Purity Perfluoroalkoxy

$IPCCAR5$ Intergovernmental Panel on Climate Change 5th Assessment Report

$IPG$ Inter-Polar Gradient

$MFC$ Mass Flow Controller

$MHV$ Melthead Gas Standard Ball Valve

$mQ$ Deionized (milliQ) water

$N_2$ Nitrogen

$NEEM$ North Greenland Eemian Ice Drilling

$NGRIP$ North Greenland Ice Core Project

$O_2$ Oxygen

$OH$ Hydroxide

$PI_g$ Gas pressure sensor

$PI_l$ Liquid pressure sensor

*ppb/ppbv* Parts per Billion (volume)

$RECAP$ REnland ice CAP project

$RICE$ Roosevelt Island Climate Evolution

$STP$ Standard Temperature & Pressure

$WS-CRDS$ Wavelength-Scanned Cavity Ring-Down Spectroscopy

$YD$ Younger Dryas

# List of Figures

# 1 Introduction

## 1.1 Gases in ice cores

Ice cores are perhaps one of the most pristine and direct records of past atmospheres present on Earth. The uniqueness of it lies in the fact that air bubbles trapped in ice cores are actual pockets of air preserved in the ice from that time period (Brook, 2007). This happens through the process of firn densification.

On the inland region of the Greenland Ice Sheet, where temperatures are almost always subzero, the annual snow layers get compressed over time as subsequent layers are deposited on top. The firn column remains porous until a depth of 80 m (in southern Greenland), allowing for diffusion of air bubbles with the surface (*CIC, Densification*). When the density reaches 800 kg/m$^3$ at approximately this depth, the pores are gradually sealed off and the air bubbles are trapped in clathrates in the ice. This part typically accounts for the lowest 10% of the firn column and is aptly dubbed the "firn-ice transition zone". A consequence of the firn diffusion zone is that the trapped air bubbles are younger than the surrounding ice; the difference is the $\Delta$age, dependent on temperature and the amount of snowfall, and can range anywhere between hundreds to thousands of years (*CIC, The firn zone: Transforming snow to ice*).

These bubbles contain important information about the concentration of greenhouse gases in the Earth's atmosphere in the past. Extracting this information can thus help us paint a better picture on what the future holds, in the context of global warming and changing climate. (Figure 1a & 1b).

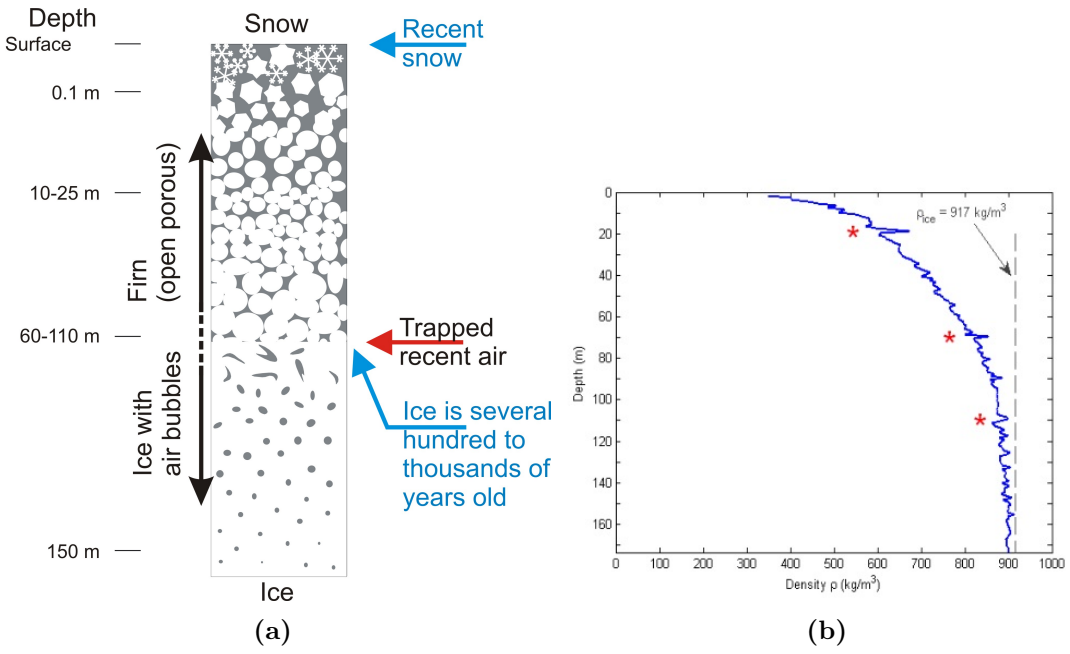


**Figure 1:** *(a) Representative depiction of the firn-ice transition zone (*CIC, The firn zone: Transforming snow to ice*). (b) Density vs Depth profile at the Dye-3 site (*CIC, Densification*)*

## 1.2 Methane

Atmospheric methane is an important greenhouse gas with a global warming potential (GWP) of 56 over 20 years (*Global Warming Potentials (IPCC Second Assessment Report)*). Although it has a lifespan on the order of 10-12 years in the atmosphere, this high potency as a greenhouse gas makes it a cause for concern.

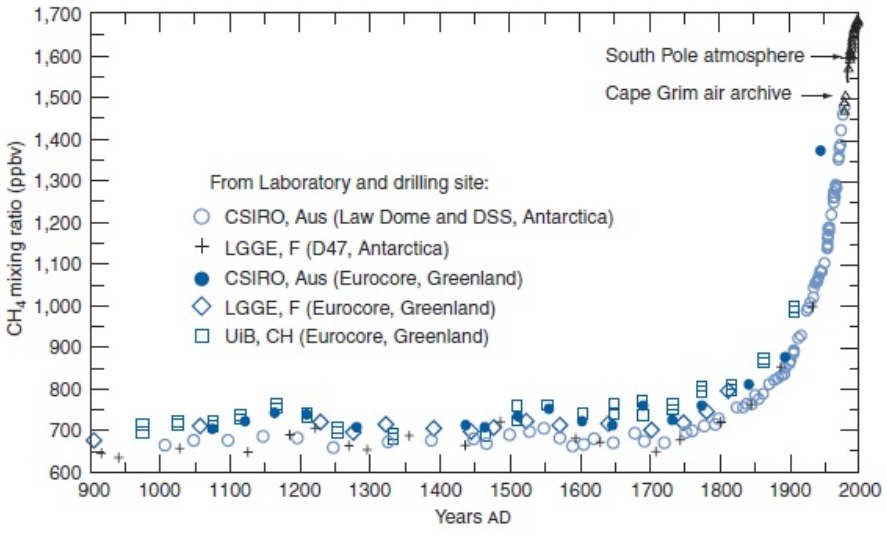


**Figure 2:** *$CH_4$ mixing ratios in the last millenium obtained from different sources in the two hemispheres (Chappellaz, 2007)*

Additionally, paleoclimatic records have shown that although methane levels have been quite consistent at 700 ppb in interglacials and 400 ppb in glacial, there was a rapid, almost exponential increase after the industrial revolution leading to an atmospheric value of 1700 ppb in the new millenium, which is around 2.5 times the normal interglacial value (Figure 2) (Chappellaz, 2007). According to the global methane budget in the IPCC AR5, anthropogenic sources contribute equally to natural biogenic sources of methane leading to a precarious balance between the net sources and sinks –of which tropospheric OH is the main sink (Figure 3) (IPCC, 2013).

Owing to its short lifespan in the atmosphere, air bubbles trapped in ice cores are one of the most pristine records of past methane. Additionally, the fast inter-hemispheric mixing rate of 1-2 years in the atmosphere, makes it an excellent chronological marker for synchronizing records from different sources and the two hemispheres (Blunier and Brook, 2001). Past methane records also indicate an inter-polar gradient (IPG), which is a quantity directly dependent on the latitudinal distribution of sources and sinks.

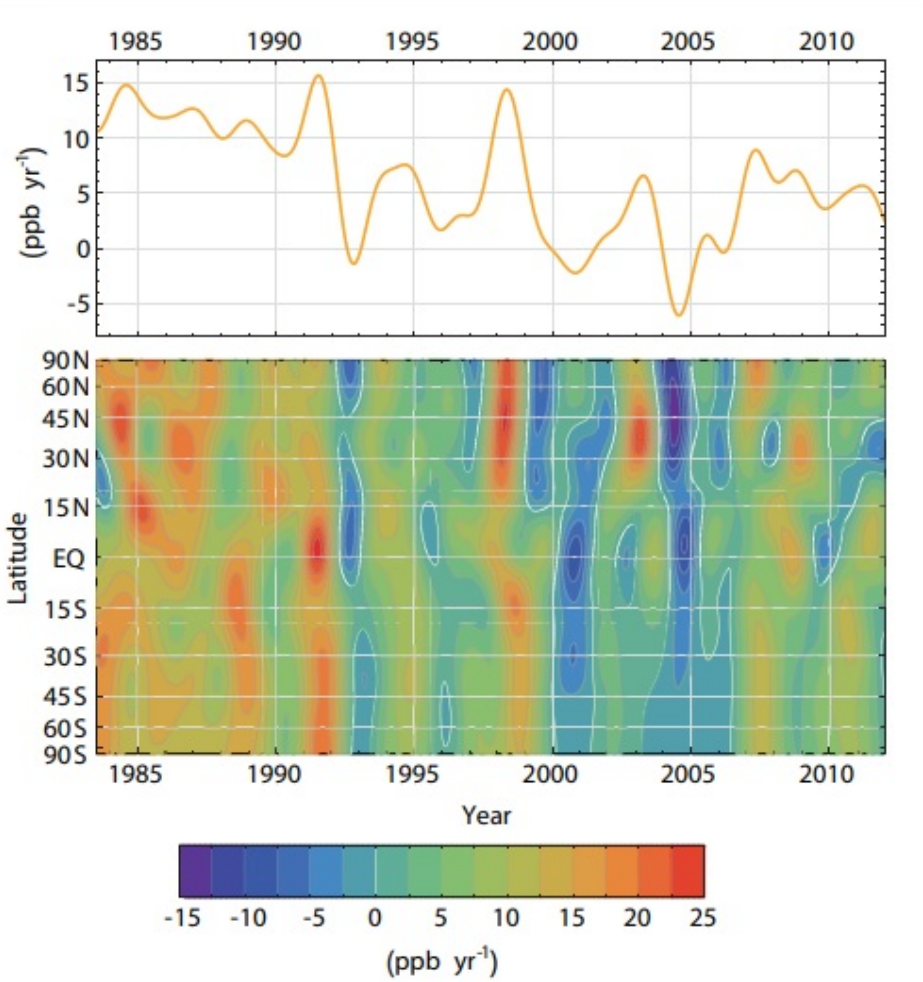


**Figure 3:** *Caption from source: "(Top) Globally averaged growth rate of atmospheric CH4 in ppb yr$^{-1}$ determined from the National Oceanic and Atmospheric Administration–Earth System Research Laboratory (NOAA–ESRL) network, representative for the marine boundary layer. (Bottom) Atmospheric growth rate of CH4 as a function of latitude (Masarie and Tans, 1995; Dlugokencky and Tans, 2013b)." (IPCC, 2013)*

Records show that the IPG has not always been constant; measurements from recent years show an IPG of 150 ppb between the northern-most and southern-most sampling latitudes (Figure 4) however; further back in time, the IPG has been as low as 15 ppb during some glacial cycles (Dällenbach et al., 2000). The addition of anthropogenic sources could explain the decreasing inter-polar gradient (IPG) observed in the recent past (Chappellaz, 2007).

It is, therefore, desirable to obtain high-resolution continuous records of methane for better synchronicity, and also to better quantify and qualify the observed IPG in methane. This will allow for a better understanding of the methane budget in the past, and also give a better idea of how that may change in the future due to the changing climate. However, it is a challenge since capturing atmospheric variability on a centennial and decadal scale requires a combined precision and accuracy of ±5 ppbv, which calls for near-absolute calibration of system parameters. With the development of the Gas-Continuous Flow Analysis (Gas-CFA) system for ice cores over the last two decades, this has now become a possibility.

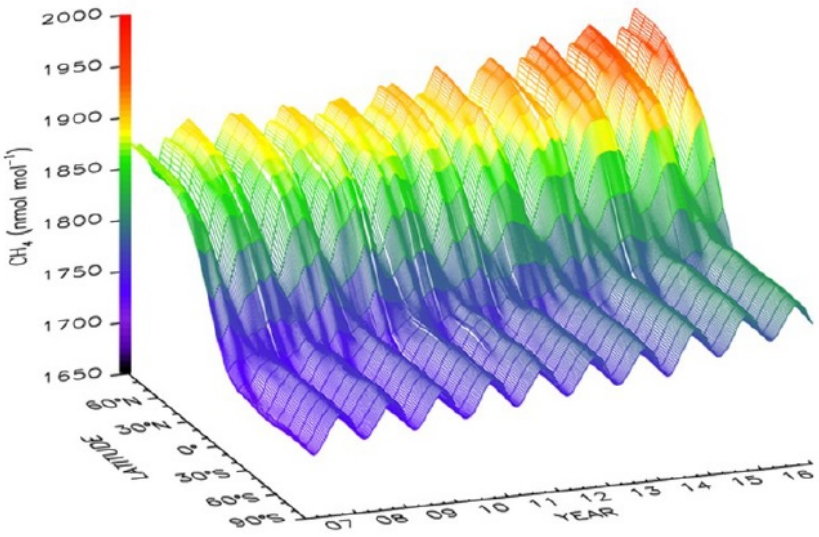


**Figure 4:** *$CH_4$ distribution over time and latitude from 2009 to 2018 (*Global Distribution of Atmospheric Methane, NOAA ESRL Carbon Cycle*)*

### 1.3 CFA system

The earliest CFA system built for analysis of wet chemistry by *Röthlisberger et al., 2000*, has then been adapted and modified over the years (e.g., Kaufmann et al., 2008; Schüpbach et al., 2009). *Schüpbach et al., 2009* was the first to develop a semi-automated system based on CFA to measure methane continuously along an ice core. This method uses gas chromatography (GC) and can provide a high resolution of 15 cm of ice that was previously hard to achieve (Figure 5).

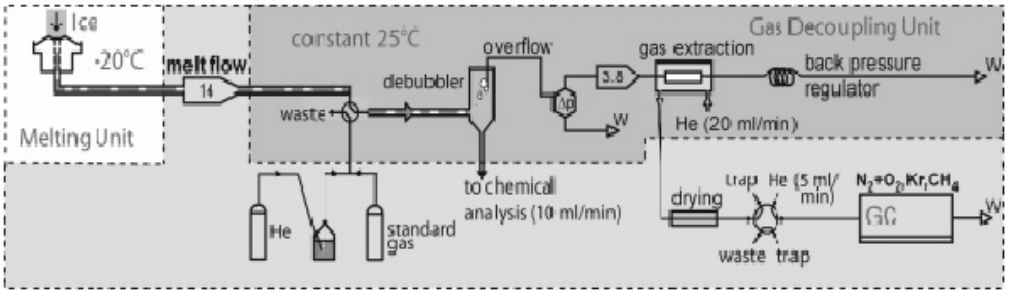


**Figure 5:** *Semi-automated CFA system with a gas chromatograph for $CH_4$ measurements (Schüpbach et al., 2009)*

Traditionally, methane measurements are done using GC; however, it is time consuming, labour-intensive and most importantly, it is a destructive method which takes away the possibility of measuring multiple gases at the same time using the CFA system (Stowasser et al., 2012). The development of laser spectroscopy for gas mixing ratios by *Güllük et al., 1997* introduced the possibility of a non-destructive, high-resolution measurement technique capable of measuring multiple gases from the same ice sample. Combined with the improved techniques of performing CFA by *Bigler et al., 2011; Stowasser et al., 2012* developed a mostly-automated, field-deployable, non-destructive method of measuring $CH_4$ and other gases from the same sample by cavity ring-down spectroscopy, using a custom-modified G1101i Picarro analyzer. This technique offers a spatial resolution of 5 cm of ice or 100 s of measurement time, with a capacity to measure 20-25 m of ice in one day (Stowasser et al., 2012).

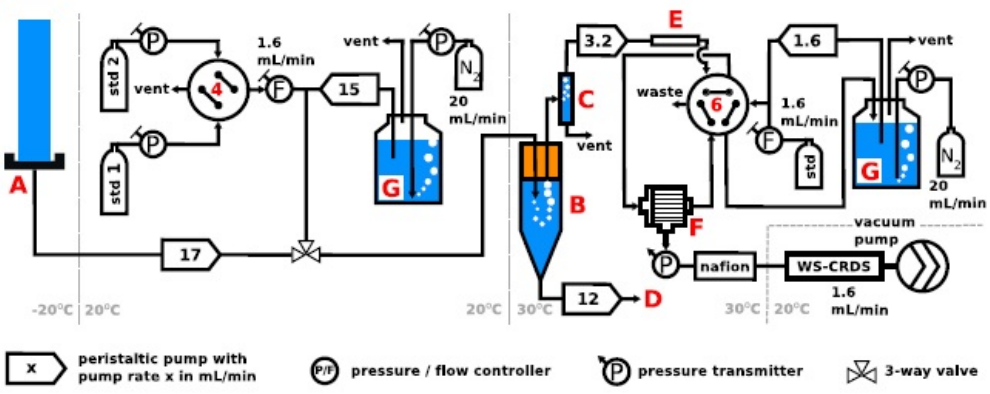


**Figure 6:** *Schematic representation of CFA set-up for $CH_4$ measurements used in the 2011 field season at NEEM (Stowasser et al., 2012)*

The technique developed by *Stowasser et al., 2012* was first used to measure the NEEM ice core using a set-up depicted in Figure 6. It has since been implemented in the measurement campaigns of the RICE and RECAP ice cores as well, evolving over time with modifications to resolve uncertainties and improve the efficiency of the system in each successive campaign. The last such variation being by *Vladimirova, 2018* (Figure 7).

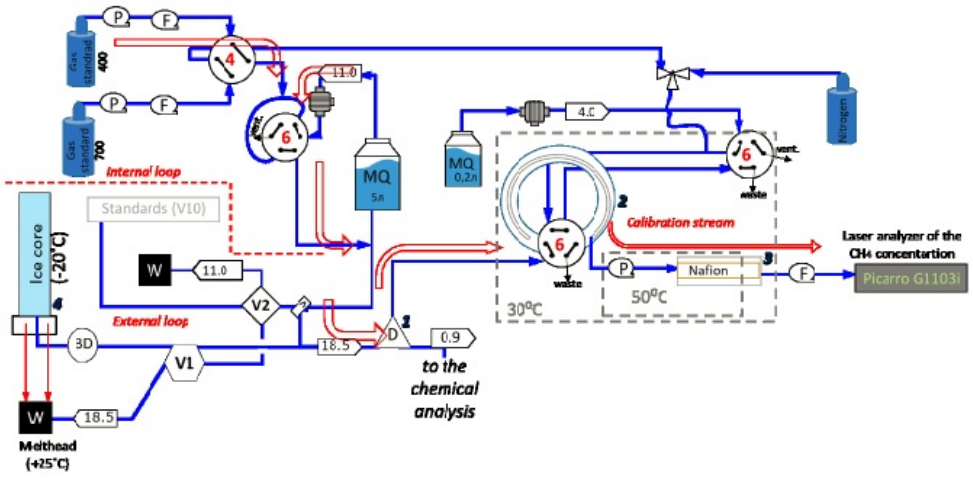


**Figure 7:** *Schematic representation of $CH_4$ CFA set-up for the RECAP ice core measurements (Vladimirova, 2018)*

The current project is also based on the same fundamental technique and still uses the custom-modified G1101i analyzer, but with modifications – some major and some minor – in order to improve the overall extraction efficiency of the system and to address some previously unresolved uncertainties. This method was implemented in the CFA of the Dye-3 ice core and the results from the campaign are presented here. Additionally, the different parameters influencing the measurements are discussed, along with suggestions for further improvements to the system in the future.

### 1.4 Dye-3

In 1979, the recently developed Danish deep drill called ISTUK was used to drill down to bedrock at the Dye-3 radar station (DYE-3 in Figure 8). The site is located at 65°11'N and 43°50'W, with an averaged annual accumulation of 53 cm ice equivalent (Dansgaard, 2004). The drilling project successfully reached bedrock at a depth of 2040 m in 1981 (*CIC, Drilling to Bedrock*).

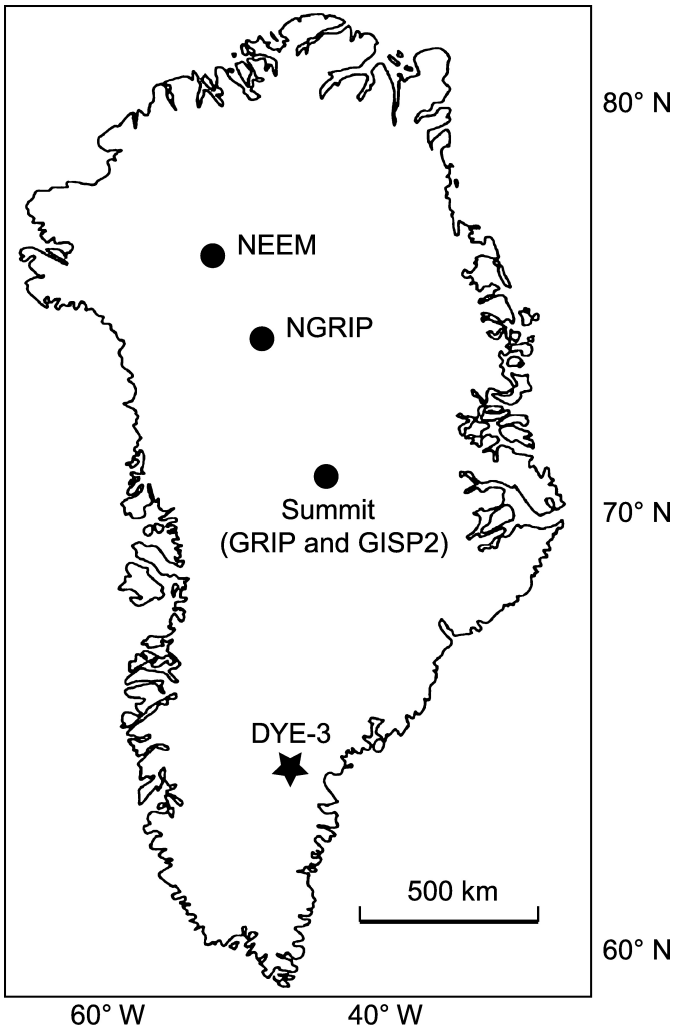


**Figure 8:** *Locations of some major ice cores drilled in Greenland, including Dye-3 (Yau et al., 2016)*

The continuous age of the Dye-3 core is estimated to be around 90,000 years; however, the last 20 odd meters of silty ice with observed basal folding, is thought to perhaps hold Eemian ice from around 125,000 years ago (Dansgaard, 2004). A recent study by *Yau et al., 2016* found the oldest average ice at Dye-3 to be 400 ka ±170 ka, predating the Eemian (Yau et al., 2016).

The Dye-3 measurement campaign in fall 2019 was a part of a larger, ongoing project to as-

similate a Greenland-wide spatial fingerprint of temperature, accumulation, and isotopic changes during abrupt climate transitions over the evolving past. The overarching goal of this project is to reconstruct the spatial pattern of abrupt climatic events over time, and reduce the uncertainty behind triggers surrounding these events, using a combination of analytical tools and modelling techniques. Dye-3 is a climatically sensitive location, where accumulation rates have increased by a significant magnitude between glacial (0.142 m/yr ice equivalent) and interglacial (0.52 m/yr ice equivalent) periods (Supplementary Information, Vinther et al., 2009; Dansgaard, 2004).

A previously unavailable, high-resolution $CH_4$ record of the entire glacial section of the Dye-3 core, along with a continuous $\delta^{18}O$ record was desired to be able to precisely constrain the $\Delta$age between the ice and the gases, in order to rightly identify sections of ice containing records of abrupt climate transitions for further isotopic studies. Due to unavailable ice for some sections, and no dedicated CFA piece allocated in the original core cut, only the bags of lengths compatible with the CFA system were measured out of all the available ice. A total of 108 m of ice was melted during the campaign, with ice expected to contain the Younger-Dryas (YD) transition, the Bølling-Allerød (B-A) transitions, and D-O events 5-11.

The focus of this thesis has been to use data from the Younger Dryas sections as an example to evaluate the functionality of the system and the robustness of the data. The effects of various system parameters and consequent data corrections have been discussed. The scope for future improvements to the system have also been identified. Evaluation of the rest of the data-set is currently underway and will be made available in the near future.

# 2 Methods

## 2.1 Set-up for Dye-3

The 1m bags of ice were cut into CFA sticks having a cross-section of 3.5 cm × 3.5 cm. The cut sticks were trimmed at breaks in the ice in the working freezer just before melting, in order to ensure minimal contamination from misalignments and gaps between pieces of ice. The melthead temperature in the warm lab freezer was maintained at 50°C, giving a melt speed of 4-4.5 cm/min on average. The length of the ice melted in unit time, was measured using an encoder, on a scale of 25 counts being equal to 1 mm of ice melted. This conversion factor was later used to reassign the depth to the data measured against time. Around 9 bags (or 9 m of ice) were measured during each melting run in one day, with 2 runs on a good day.

The segmented flow of liquid and gas bubbles from the melthead passed through a 4-port switch valve ('Melthead valve' in Figure 10) and was pulled by a peristaltic pump set to a speed of 23 ml/min. A triangular debubbler was then used to extract a small fraction of sample (3-4 ml/min) for dust measurements. The remaining bulk of the sample stream was made to pass through a 20 µm particle filter, to ensure that particles from the dusty glacial ice did not clog the extraction membrane. The use of a manual 6-port valve ('Filter Swap valve' in Figure 10) made it possible to swap between two filters, enabling uninterrupted flow of sample when the filter had to be changed. Typically, the filter was replaced on a daily basis; however, liquid flow measurements were also a good indicator of when the filter needed to be changed, in case there had been a particularly dusty section of ice.

Once the majority of the larger dust particles were removed, the sample passed through a 6-port switch valve ('Bypass valve' in Figure 10) to reach the micromodule. A 0.75" X 1" membrane module ('Micro Module' in Figure 10), consisting of small, closely-packed, microporous, hydrophobic hollow fibre membrane arrays in parallel packing configuration , was used as the main gas extraction unit. The shellside volume of the membrane is 6.5 ml and it can operate with liquid flows from 15-200 ml/min (*3M, Liqui-Cel MM-0.75X1 Series Membrane Contactor*). The module was oriented vertically for preferential ease of gas flow. Since these modules are typically meant for deagssing and not for extraction, no regular tubing connections were possible on the sample liquid inlet opening on the module's shellside for direct contact with the membrane interface as would have been preferred. This was worked around by making a makeshift tubing connection by fitting a 1/8" HPFA tube through a softer plastic tubing having 1/8" inner diameter, which could be squeezed into the shell in a way that was leak tight (Figures 9a & 9b).

The gas extraction was facilitated by using a Back Pressure Regulator (BPR) (EL-PRESS P-702CV (P1 CONTROL), Bronkhorst) at a setpoint of 300 mbar, creating a pressure gradient of 700 mbar across the extraction unit. Since the pressure difference from the liquid phase is the main driver for gas permeation through the membrane, having a high and constant pressure gradient created stable conditions that significantly improved the extraction efficiency. The setpoint of 300 mbar was chosen as optimal following a series of multivariate tests to deduce the dependency of extraction efficiency of the module on liquid flow rate, gas flow rate, pressure gradient, and gas percentage in the ice. The need to have a stable and higher pressure than the mass spectrometry unit, which was an under-pressure system maintained at 200 mbar using a second BPR, was an additional deciding factor in choosing the pressure gradient across the module.

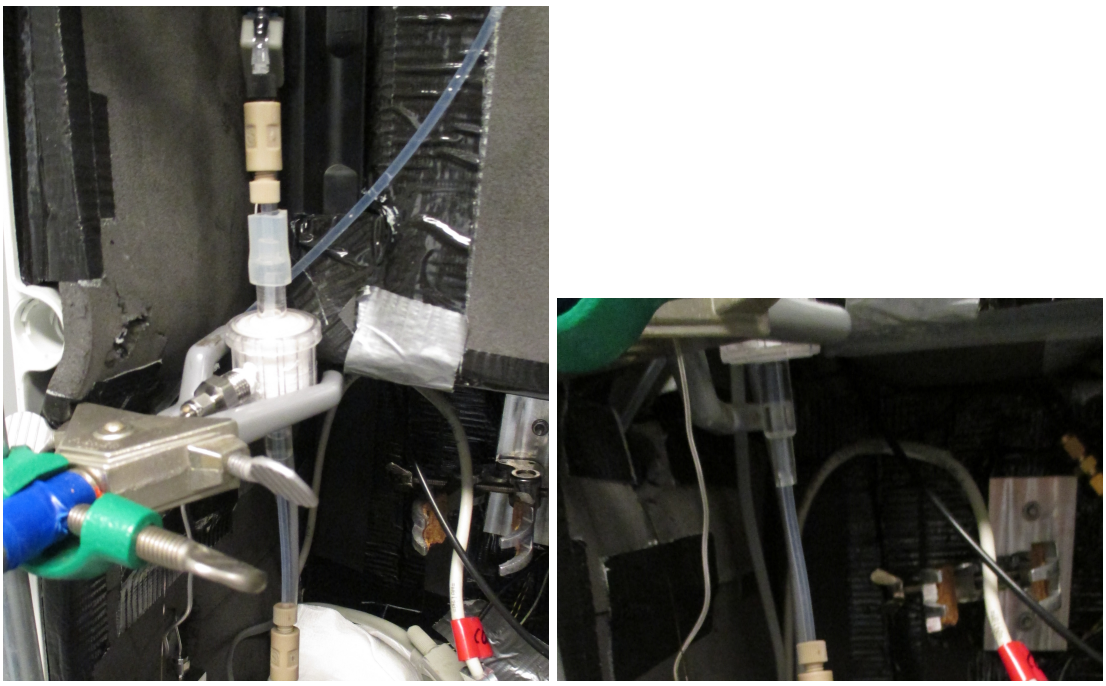

**(a)** **(b)**

**Figure 9:** *(a) Picture of the micromodule set-up for the campaign. (b) Picture of tubing connections to the micromodule in the set-up.*

Two liquid pressure sensors (26PCBFG5G, Honeywell) were used to measure the pressure at the inlet and liquid outlet of the micromodule respectively. Two Sensirion LS32-1500 Liquid Flow Meters were used to measure both the actual amount of sample extracted for dust measurements, as well as the flow rate at the liquid outlet of the micromodule, before it was sent for further wet chemistry analyses. From the extracted gas, a constant flow of 0.15 ml/min was sent to the mass spectrometry unit for measurement of nitrogen and argon isotopes in the ice. The bulk of the gas stream was measured by a GE UNIK 5000 pressure gauge, before being dehumidified using a Nafion membrane of length 1.28 m encased in a 1/8" steel coil (TT-030, Nafion, Perma Pure). It is a semi-permeable membrane that selectively removes water vapour from a gas mixture. A purge flow of 30 ml/min of $N_2$ was used as a carrier for the removed water vapour. The Nafion dehumidified the sample gas stream to less that 0.1% volume water vapour, which negated the need for water vapour corrections in the Picarro measurements. A 1.84 m long capillary having an inner diameter of 530 µm connected the Nafion to a high-precision gas flow meter having a range of 10 ml/min STP ('FIg' in Figure 10) (LOW-ΔP-FLOW F-100D, Bronkhorst). A Picarro G1101i trace gas analyser was used to measure the mixing ratio of CH4 in the known sample flow, using Wavelength-Scanned Cavity Ring-Down Spectroscopy (WS-CRDS) at a cavity pressure of 45 Torr. The analyser used is customized for small sample volumes having a small cavity volume of 9.6 cc, with an effective internal volume of 0.57 ml at 45 Torr (Stowasser et al., 2014) . The small cavity volume in conjunction with a lower operating pressure, enabled measurements at higher resolution, allowed a higher pressure gradient across the extraction unit, and better overall efficiency of the system.

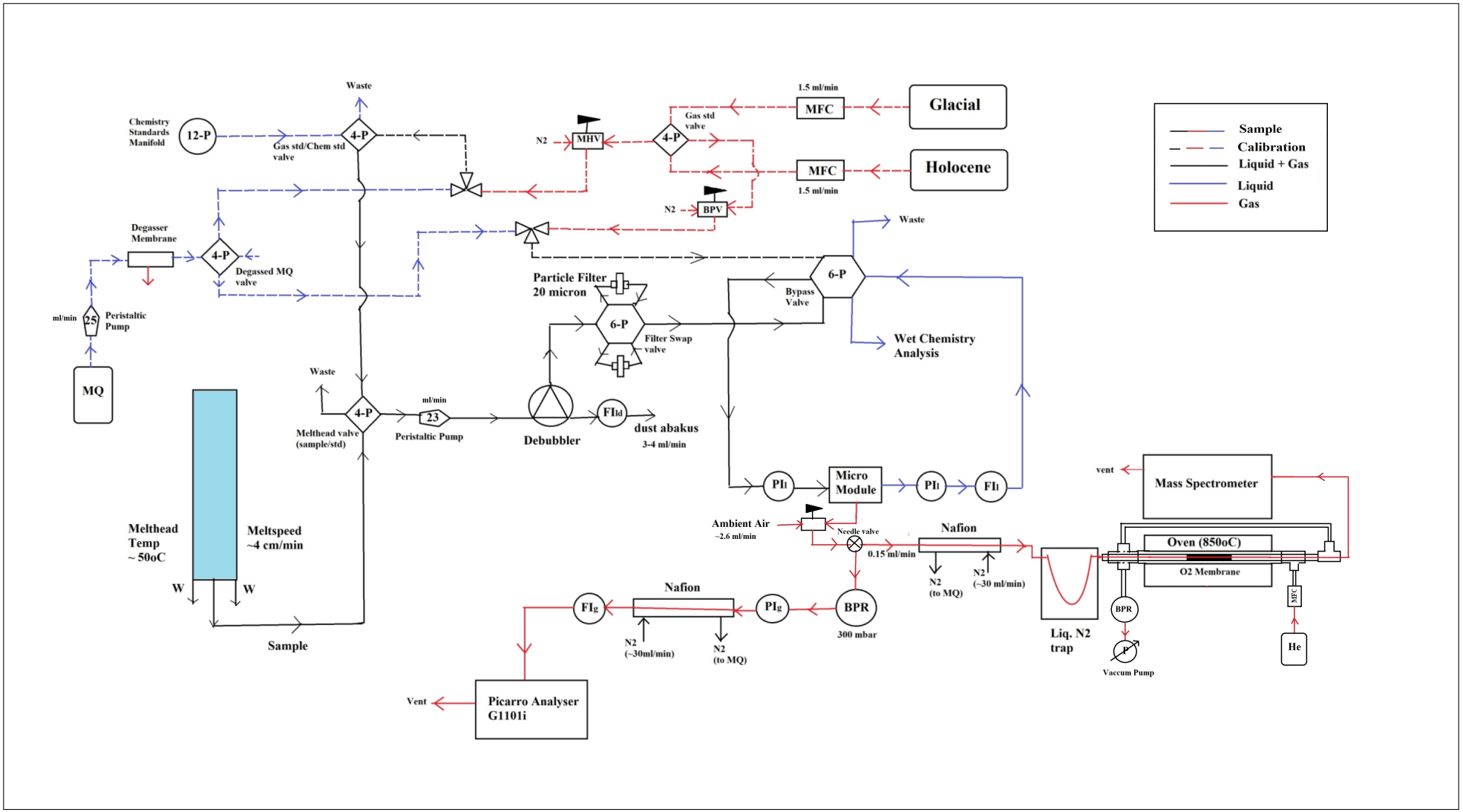


**Figure 10:** *Schematic of CFA set-up for the Dye-3 campaign*

## 2.2 Calibrations

### 2.2.1 System

1. **Daily calibrations** The Melthead valve allowed the option to switch from sample stream to Chemistry/Gas standard stream to perform calibrations. Daily calibrations were carried out thrice a day; once in the morning, once in between the runs and once at the end of the day. A 4-port switch valve ('Gas std valve' in Figure 10, C4WMPH, VICI AG) was used to switch between the two gas standards - Glacial and Holocene. The gases were pre-made mixtures of $CH_4$, $N_2$, and $O_2$ with methane mixing ratios of 403.1 ppbv and 701.2 ppbv respectively (Stowasser et al., 2012). The flow of the chosen standard gas was set to 1.5 ml/min regulated by a Mass Flow Controller (MFC) (GM50A, MKS Instruments Inc.) and used to simulate the sample stream by creating a segmented flow with deionized (mQ) water (Millipore Advantage, 18.2 MOhm $cm^{-1}$) pumped from a 5L glass bottle. The mQ water was continually degassed with $N_2$ from the combined purge flows of the two Nafion dryers. A larger hydrophobic membrane degasser unit accepting liquid flows up to <500 ml/min ('Degasser Membrane' in Figrue 10) (3M Liqui-Cel MM-1X5.5 Series Membrane Contactor) was used to further degas the mQ water before creating the mQ + gas mixture using a simple T-P connection. When the 'Gas std/Chem std' valve (Figure 10) was set to 'Gas std', this stream of mQ + gas was allowed to flow through the whole system, passing through the 'Melthead valve'. Each standard gas was run for 15 minutes in turn during one calibration run. Once calibrations were done, a mixture of mQ water + Glacial standard, at a flow of 1.5 ml/min, was made to flow through the system before melting commenced. The low methane mixing ratio of the Glacial standard significantly minimized the effect of the initial contamination spike from the mQ ice at the start of every run.

   A ball valve ('MHV' in Figure 10) before the T-P allowed the option of switching between a standard gas or $N_2$ gas to be sent to the 4-port 'Gas std/Chem std' switch valve. The unused gas was also controlled by an MFC and sent to another ball valve ('BPV' in Figure 10), also provided with the option of switching to nitrogen. During chemistry standard runs, the Bypass loop in the 'Bypass valve' was activated, which isolated the gas side of the set-up. A mixture of the gas from the BPV, and deionized (mQ) water from the bottle were passed through the micromodule (with the liquid outflow going to waste), ensuring that the gas system never ran out of flow and was maintained at stable operating conditions at all times.

2. **Time Delay** The response time of the system was estimated as a sum of time taken for the sample (liquid + gas) to reach the micromodule from the melthead, and the time taken for the extracted gas to then reach the picarro from the micromodule.
   1) ***Melthead to MicroModule*** - The first bag of ice during each run was preceded by a 7 cm block of mQ ice; however, sample measurements started mid-way through the melting of the mQ ice. Since the mQ ice contained little gas, there was always a pressure drop observed while melting the mQ ice which then led to a sudden pressure surge at the BPR indicating sample volume build up at the micromodule. The time taken from the start of the melting for this spike to occur, combined with the total flow rate that was measured, allowed for an estimated internal volume of 12 ml STP in this section.

2) ***MicroModule to Picarro*** - The estimation of internal volume in this part of the set-up was corroborated by different methods. Firstly, during melting, it was observed that a contamination spike was always preceded by a pressure spike at the BPR corresponding to a pressure spike in the cavity. There was then a further delay before the peak of the methane data fit in the analyser started to shift from stable values. Emperical data, on delay times between when a break in ice was observed to when a pressure spike at the BPR was observed and when the methane peak shifted, was collected over the course of the campaign, and found be approximately consistent. Furthermore, a series of tests were done by alternatively switching between the two standard gases at varying flows. Once again, a pressure spike was observed at the cavity corresponding to the change in gas, right before the methane fit peak started shifting from the stable values for that standard (Figure 11). This difference in time, combined with the gas flow rate at that point, was used to estimate the internal volume in this part of the set-up using gas flow rates ranging from 0.9 to 1.5 ml/min with 0.1 ml/min interval increases. The average internal volume from these tests was determined to be 10.93 ml for this section of the system (Appendix III).

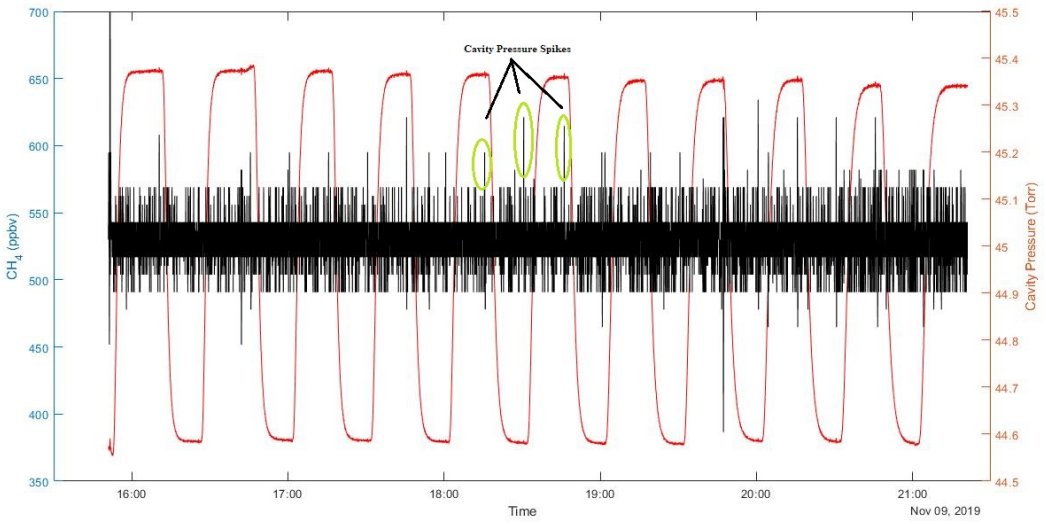


**Figure 11:** *Plot showing $CH_4$ data with cavity pressure plotted on top. Examples of all identifiable peaks between 18:00 and 19:00 hrs are marked in green.*

Knowing the volumetric flow rate of the sample, and corresponding liquid and gas pressures at every point in time, made it possible to then estimate the volume of sample at STP for every point in time as a function of pressure and flow. The volumes were cumulatively summed and at the point at which it was closest to the estimated internal volume at STP, the cumulative sum of measurements in unit seconds were added up to find the delay for that particular sample measurement. The slight overshoot that occurred since the cumulative sum is never exactly the estimated internal volume, was corrected for. The total delay time was taken as the sum of the delay time from melthead to micromodule (liquid+gas sample) and micromodule to Picarro (gas sample). The estimated times were verified by implementing them in the depth scale and comparing whether contamination spikes in the data lined up where expected at marked breaks in ice.

### 2.2.2 Picarro

There exists an offset in measurement caused by operating the analyser at a low cavity pressure, possibly due to the analyzer not being properly calibrated at lower operating pressures. Additionally, low flows also impacted the measurement, with the Picarro overestimating methane mixing ratios at lower flows. In order to correct for these measurement errors, it was necessary to perform calibrations by directly running only the pure standard gas into the cavity over a range of flows. To make this feasible, a temporary connection was made by replacing the 'Ambient Air' connection (Figure 10) to the ball valve before the BPR by a steel tubing connecting directly to the 'Gas std valve'. This gas was then dehumidified using the Nafion dryer and the flow rate was measured using the FIg, before being sent to the Picarro. The MFC was used to vary the flow over the range of 0.5-2.75 ml/min, with 0.25 steps in between. The gas at each flow rate was run for 15 minutes and the average measurement of the last 10 minutes were taken to be the true measured value. This was done for both the Holocene and the Glacial standard gases. A common correction factor dependent on measured $CH_4$ and the flow rate at $FI_g$ was derived by combining the results from the two standard gases.

### 2.2.3 Module

A set-up resembling the 'Bypass' loop in the final set-up was used to calibrate the extraction efficiency of the module as a function of pressure, flow and gas percentages (defined as $\frac{GasFlow}{LiquidFlow+GasFlow} \times 100$). The expected total flow was aimed at simulating the main melthead pump, which pumps the segmented sample flow of liquid + gas. It was found to be not possible to pull the gas + liquid mixture through the peristaltic pump, possibly owing to the large dead volume posed by the main Degasser Membrane for the mQ water. Therefore, the degassed water was pumped to a T-P connection where the standard gas was then added using a capillary (320 µm inner diameter) going into the 1/8" HPFA tubing. For every fixed point of expected total flow at 18, 20, 23 and 25 ml/min respectively, the gas flow and liquid flow were varied corresponding to gas percentages of 7, 9, 10, 11, 13, 15 in the total flow by changing the pump speed and MFC setpoint accordingly to always reach the expected total flow. For example, for an expected total flow of 25 ml/min with 10% gas, the gas flow was set to 2.5 ml/min at the MFC and the liquid flow was set to 22.5 ml/min at the peristaltic pump. At flows corresponding to each percentage gas, the pressure gradient was varied from 500 to 750 mbar in 50 mbar steps, by changing the set-point of the BPR from 250 to 500 mbar. A high-precision gas flow meter (FIg) was used to measure the extracted flow. Measurements in each setting combination were done for 5 minutes, using the last 2 minute average as the stable value. All measurements were done at a constant temperature of 30°C and using $N_2$ gas.

## 2.3 Data Correction

A semi-automated MATLAB code (MATLAB, ver. R2019b) was written to convert the raw encoder data into melt rates, which were then used to calculate a raw length of ice measured for every run. During the frame changes in a run, the encoder was disconnected in order to stack the next frame of ice, which meant a loss of encoder data during these intervals, even though the ice continued melting. In order to interpolate across these intervals, the code made it possible to manually choose the threshold values of the encoder below which the data had to be interpolated. The missing ice at breaks in a bag and between bags were included based on the CFA freezer cutting logs. A time delay, calculated according to **Section 2.2.1.2**, was then added to the depth scale in order to correlate the $CH_4$ data from the Picarro measurements. The mean gas flow for each bag was calculated as a sum of the mean flow measured by the $FI_g$ for the bag, a constant 0.15 ml/min of flow to the mass spectrometer, and 10% of the liquid flow extracted for the dust measurements before gas extraction. The gas% for each bag was then calculated as the mean gas flow for each bag being a fraction of the mean total flow for each bag, including the liquid flows. The raw Picarro data was first set on the delay-corrected depth scale and screened for repetitive values, which were replaced by NaNs. Following that, cavity pressure and flow offset corrections were applied. The depth scale was then aligned with field logged measurements, and contamination spikes were removed in order to get the final $CH_4$ (ppbv) vs Depth (m) data for each run.

# 3 Results

## 3.1 Module

For all combinations of setpoints based on varying the gas percentage in flow, the module consistently performed better at low BPR setpoints (or higher pressure gradient with the liquid phase) (See Appendix I). The extracted flow consistently decreased with decreasing pressure gradient. Note that there was no liquid pressure measurement from the liquid outflow of the module during these experiments. But since there are no restrictions along the liquid line, the pressure has been approximated to be atmospheric. Figure 12 is an example of measured flows corresponding to varying BPR setpoints for 10% gas in an expected total flow of 23 ml/min.

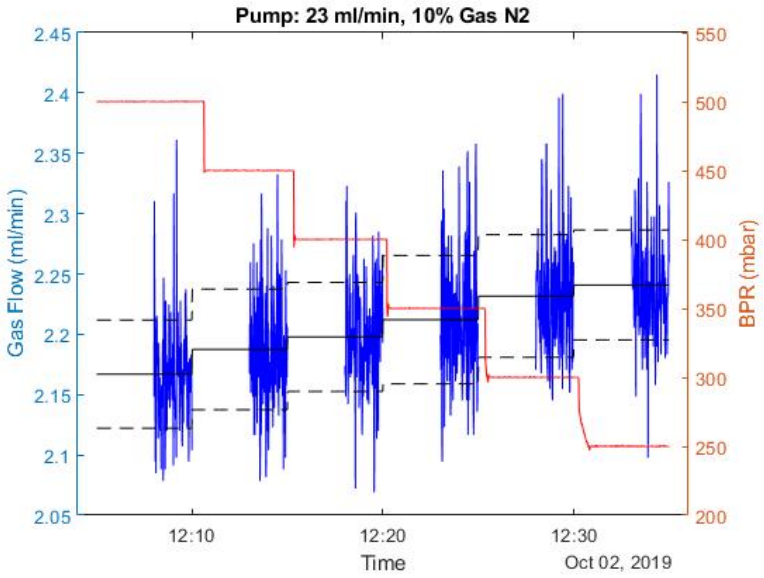


**Figure 12:** *Measured gas flows extracted from the micromodule at varying BPR setpoints at 10% expected gas flow. '—': Mean value, '- -': Std deviation.*

The extraction efficiency for every run was calculated as,

$$E_{eff} = \frac{FI_g}{MFC}$$

$E_{eff}$ = Extraction Efficiency of module

$FI_g$ = Measured gas flow

MFC = Mass Flow Controller set-point

Since all measurements were done with the melthead pump set to 23 ml/min and the BPR set to 300 mbar, it was especially interesting to see how the module behaved under those specific conditions for different % gas flows. From Figure 13a, low percentage gas flows seem to be most affected in terms of decreasing pressure gradient on the order of a 5% decrease in extraction efficiency. For very high gas percentages, this slope is not as pronounced, leading to a seeming decrease of 1.5% in extraction efficiency going from 250 mbar to 500 mbar BPR set-point. Since the gas flows in the Dye-3 core fell within a range of around 7% gas in the ice, it was imperative to operate with as high a pressure gradient (or as low a BPR set-point) as possible, to facilitate maximum extraction.

From Figure 13b, it appears as though the maximum extraction efficiency was not achieved by having a combined flow of 23 ml/min. However, it was a trade-off between that and the benefits of melting faster and allowing lesser time for dissolution in the system. Moreover, between the lowest and highest percentage gas in a flow of 23 ml/min, the decrease in efficiency is only on the order of 1%.

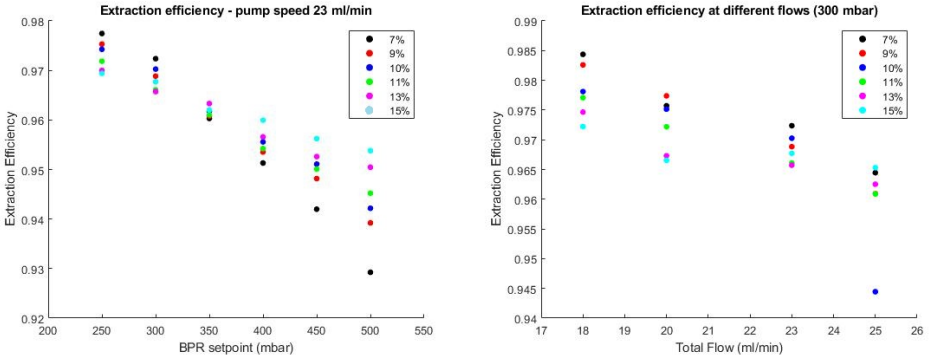


**(a)** **(b)**

**Figure 13:** *(a) Extraction efficiency of the module at different BPR setpoints for different gas percentages for an expected total flow of 23 ml/min. (b) Extraction efficiency of the module at 300 mbar BPR setpoint for different gas percentages and different expected total flows*

Although the aim was to simulate the flow of the melthead pump in these measurements, it was not possible to pull the combined flow of gas+liquid with the peristaltic pump. As mentioned in **Section 2.2.3**, this is possibly owing to the large dead volume created by the main Degasser Membrane for the mQ water. The pump was set to the desired liquid flow rate corresponding to the gas percentage, which determined the gas flow added from a MFC through a capillary. This resulted in slightly higher gas percentages actually measured from the flow and slightly lower liquid flows than anticipated from the pump since the measured combined flow did not accurately represent the desired total flow (see Appendix I). Table 1 shows the gas percentages from the actual measured total flow, calculated as

$$Gas\% = \frac{FI_g}{FI_g + FI_l} \times 100$$

$\mathrm{FI}_g$ = measured gas flow (ml/min)

$\mathrm{FI}_l$ = measured liquid flow (ml/min)

At the range of around 7% gas in the ice as measured along the Dye-3 core, it can be said that the extraction efficiency of the module is around **97%**.

**Table 1:** *Extraction Efficiency at measured Gas % for expected total flow 23 ml/min at 300 mbar BPR setpoint*

| Measured Gas % | Extraction Efficiency |
|---|---|
| 8.23 | 0.9724 |
| 10.39 | 0.9688 |
| 11.46 | 0.9703 |
| 12.40 | 0.9661 |
| 14.57 | 0.9657 |
| 16.60 | 0.9677 |

### 3.2 Picarro

While calibrating for the cavity operating pressure offset from the true value of methane by measuring dry standard gas through the system, it was found that the Picarro overestimated the $CH_4$ mixing ratio at lower flows (Figures 14a & 14c). Between the lowest and highest flow rates measured, the difference in mixing ratio was on the order of around 8 ppbv and 7 ppbv for Glacial and Holocene standards respectively. To determine the expected measured values, the measured $CH_4$ was plotted against the inverse flow for both standards, taking the intercept of the fit (Browaeys, 2020) as the stable expected value of methane (Figures 14b & 14d). This was done since both the Glacial and Holocene measurements tended towards stable values at higher flows, making the intercept when plotted against inverse flow, the most stable value expected, tending towards $\infty$.

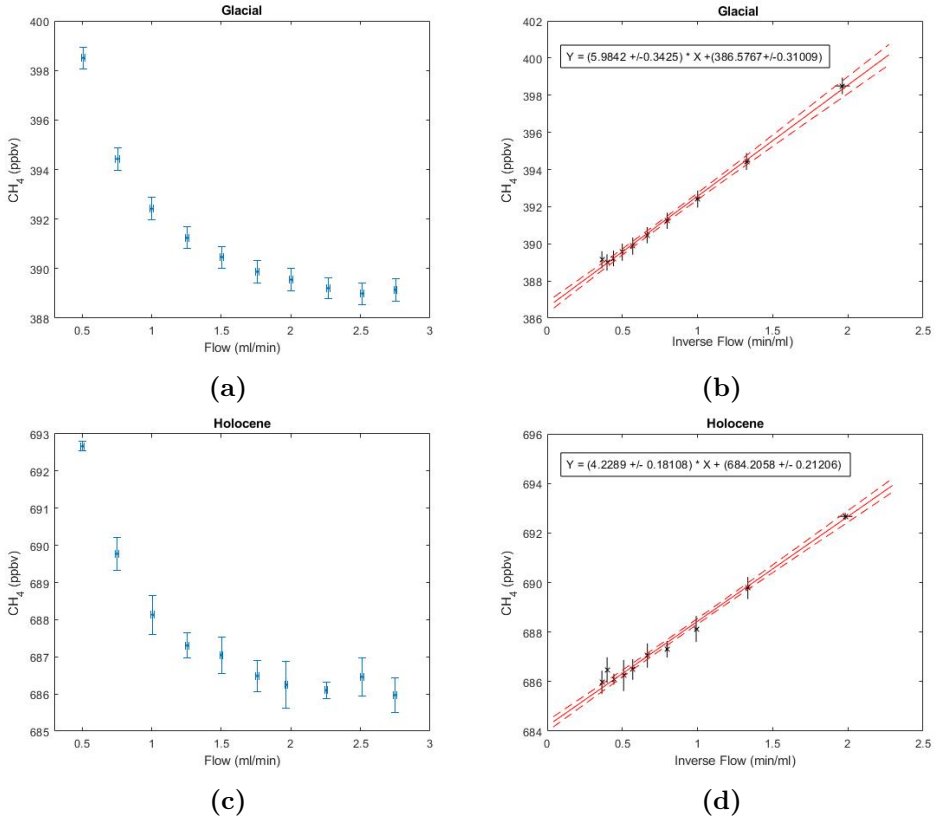


**Figure 14:** *(a) $CH_4$ vs Flow for dry glacial standard to Picarro (b) Fit line for $CH_4$ Glacial vs inverse flow (c) $CH_4$ vs Flow for dry Holocene standard to Picarro (d) Fit line for $CH_4$ Holocene vs inverse flow*

From both these fits, it can be extrapolated that,

$$CH_4 = S \cdot \frac{1}{FI_g} + CH_{4int} \tag{1}$$

$CH_{4int}$ = intercept value

S = Slope of fit

Plotting the intercepts vs the true values of the standards (Figure 15), we get the relationship,

$$CH_{4int} = m \cdot CH_{4true} + c \tag{2}$$

m = slope of fit

c = intercept from fit

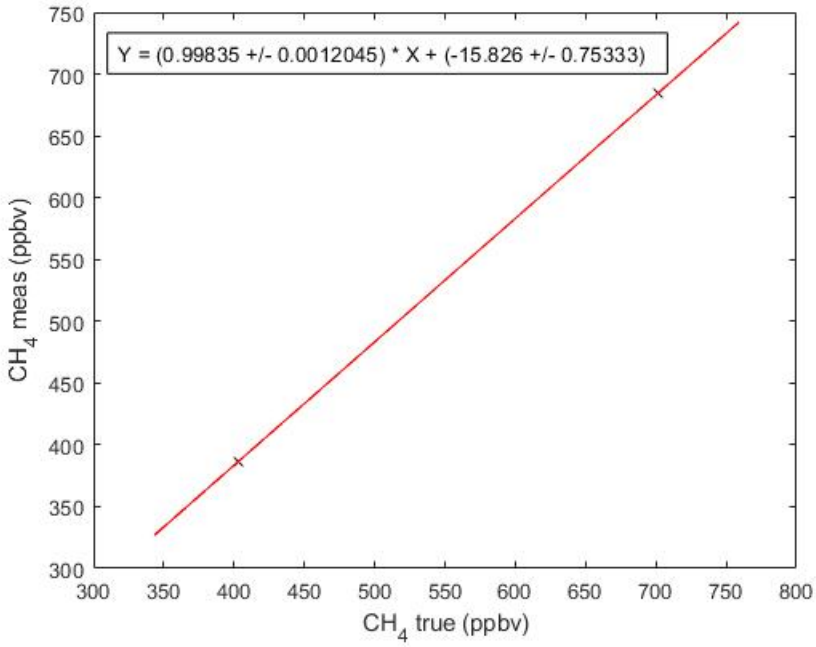


**Figure 15:** *$CH_4$ meas (here read: $CH_{4int}$ from Figures 14b & 14d) vs $CH_4$ true for the two standard gases*

However, since both standard measurements exhibited significant flow effects, the slope S first needed to be expressed as a function of the intercept value in order to determine a common correction factor for measured $CH_4$ mixing ratios. Therefore, the slopes obtained from Figures 14b & 14d were plotted against the respective intercepts and a linear fit was performed using linfitxy (Browaeys, 2020) to obtain a relationship between slope and individual fit intercepts (Figure 16). This gave the slope as a function of intercept,

$$S = S_{slope} \cdot CH_{4int} + S_{int} \tag{3}$$

S = slope in (1),

$S_{slope}$ = slope from Figure 16,

$S_{int}$ = intercept from Figure 16

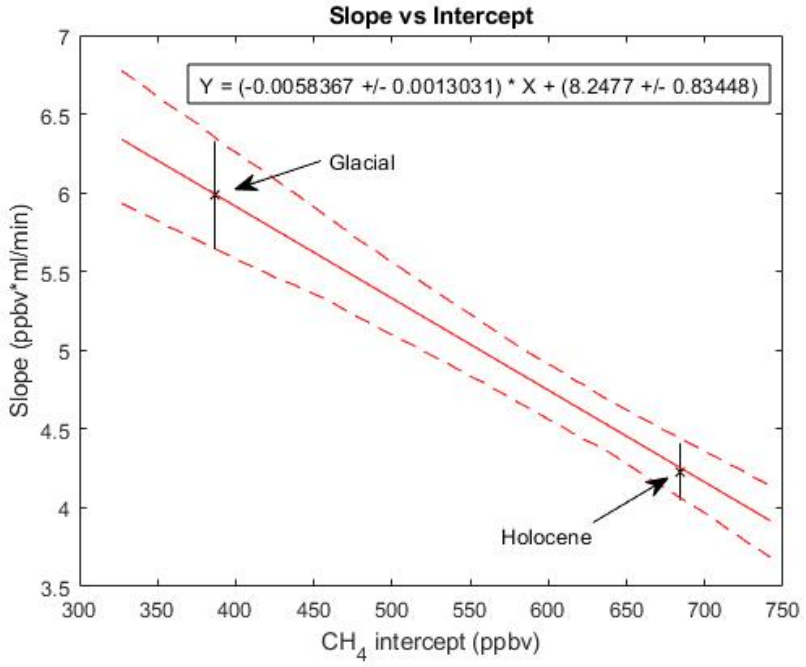


**Figure 16:** *Fit line for Slope vs Intercept from Glacial fit and Holocene fit*

Substituting in equation (1) and reducing, we get,

$$\boxed{CH_{4int} = \frac{CH_{4meas} - \frac{S_{int}}{FI_g}}{1 + \frac{S_{slope}}{FI_g}}} \tag{4}$$

where $CH_{4meas}$ is the raw measured data from the Picarro. The $Ch_{4int}$ value thus obtained can be used in equation (2) to get the true value of the methane mixing ratio ($CH_{4corr}$),

$$\boxed{CH_{4corr} = \frac{CH_{4int} - c}{m}} \tag{5}$$

All errors were propagated to get an uncertainty as a function of $FI_g$ and $CH_{4meas}$ for each individual measurement.

## 3.3 $CH_4$ on a depth scale

### 3.3.1 System corrections

The encoder data was first converted to a melt rate vs time scale using a conversion factor of 25 encoder counts = 1 mm. The melt rate was obtained in units of cm/min. The raw depth at each point was then calculated as the melt rate at that point in unit seconds. Missing ice was added at breaks in bags, and between bags in order to obtain the actual depth of each bag in a run at that point in time (Figure 17). Due to the need for interpolation across frame changes where the encoder measured 0 counts even though the ice was melting, it is probable that some discrepancies are introduced. However, a bag offset was calculated for each bag as the difference between the CFA freezer measured length and the calculated length of each bag from the code. Thus, it was possible to verify that the error from freezer measurements was constrained to less that 1% in most cases, with the worst of the outliers being an error of 2% of the corresponding actual bag length. The total accumulated error in calculated length of all the ice measured in the campaign was found to be **-0.0564 m** (negative indicating calculated length was longer), which amounts to a total calculated length 5.27% longer than the cumulative length of 108 bags of ice, and thus deemed an acceptable error for the present data analyses (see Appendix II).

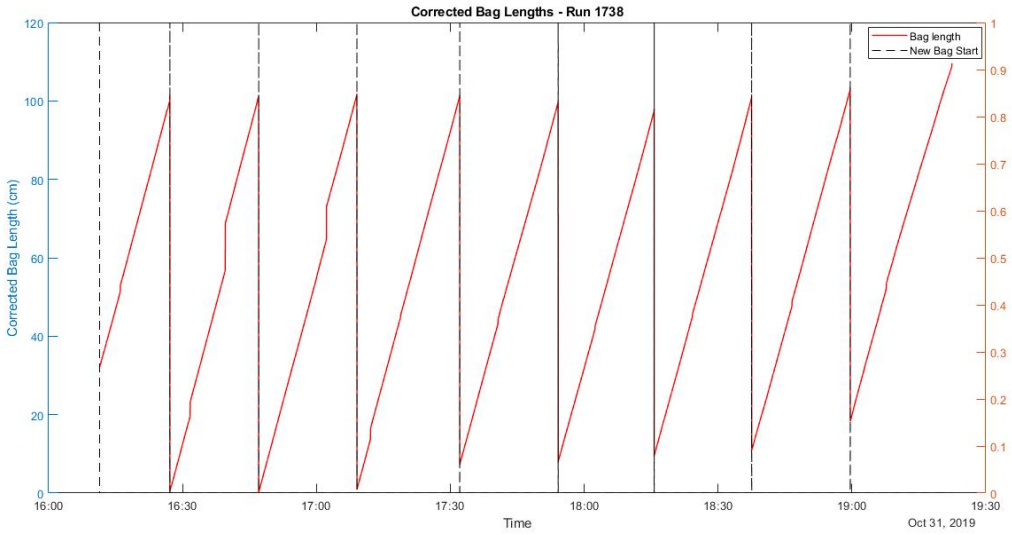


**Figure 17:** *Bag lengths for Run 1738 with missing ice added*

For each run, the bag mean gas flow and bag mean gas% in flow was calculated (Figures 18a & 18b). The varying gas flow meant that the delay times to the instrument were not constant and had to be computed for each data point individually as described in **Section 2.2.1.2**. Using Boyle's law for relating between changes in volume and pressure in the system compared to STP, the volume at each point was defined as a cumulative sum of gas volume under measured pressures until the estimated volume at STP was reached. The time taken for this was then assumed to be the delay time to the instrument for that point of measurement.

$$p_g \cdot v_g = P \cdot V \cdot t \tag{6}$$

$p_g$ = pressure of gas in system (mbar)

V = volumetric flow rate of sample gas (ml/min, STP). NOTE: This is because the $FI_g$

measures in volumetric units at STP

t = time in minutes

P = pressure at STP (mbar)

$v_g$ = volume of gas in the system (ml)

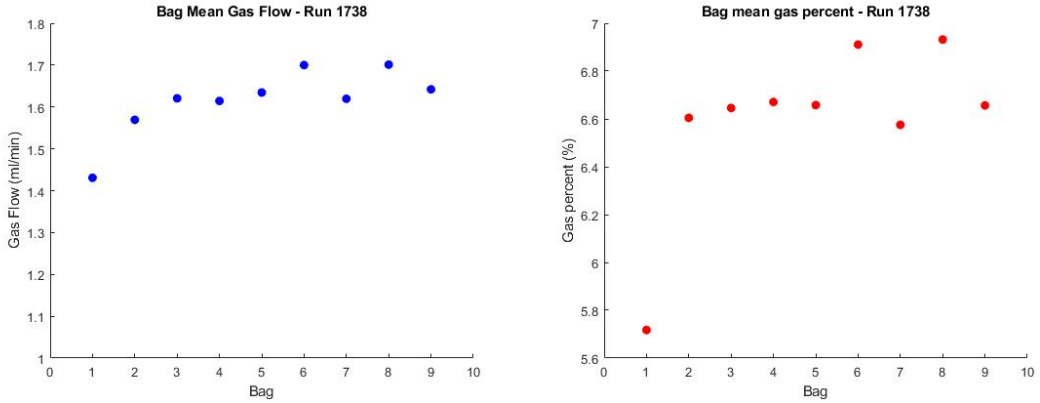


**(a)** **(b)**

**Figure 18:** *(a) Mean gas flow per bag in run 1738 (b) Gas% per bag in run 1738 from measured flows*

Once the delay corrections were applied to the depth scale, corrections were also made for the instrumental offset caused by lower flows and the insufficient analyser calibrations at lower operating cavity pressures. Figure 19 shows the data corrected for these offsets. The actual correction factor is dependent on each individual measurement and flow, and the errors associated with them, as expressed in **Section 3.2**. However, to give a general idea of the significance of this correction, the mean correction factor for Run 1738 (Figure 19) is **+13.05 ppbv** with a mean error of ±1.36 ppbv.

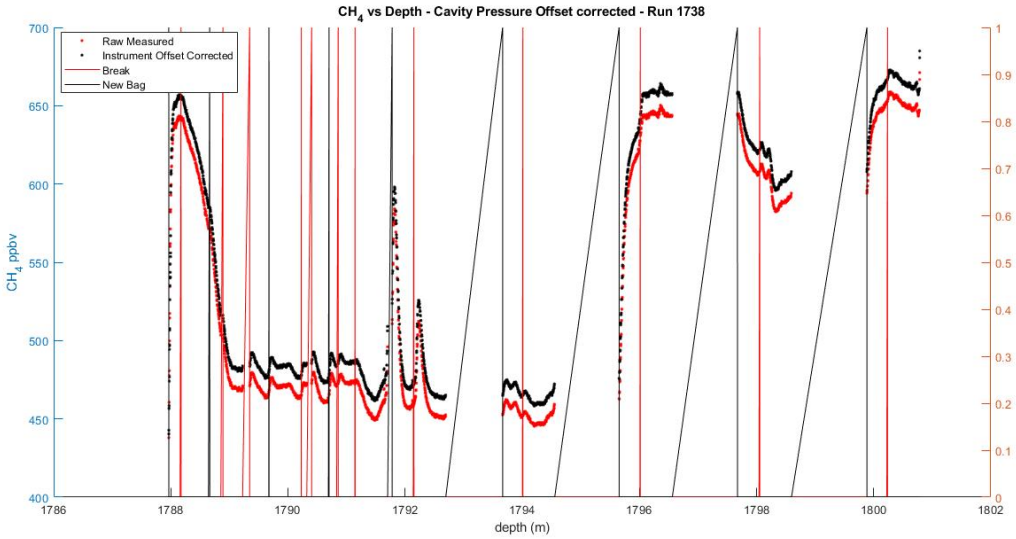


**Figure 19:** *$CH_4$ vs Depth corrected for time delays and cavity pressure offsets*

### 3.3.2 Uncertainties from ice

Upon comparison of CFA freezer measured bag lengths to the actual field log from 40 years ago, it was found that the new length measurements did not match, and were oftentimes longer. The majority of the bags have an offset in the range of 1-10% (Figure 20).

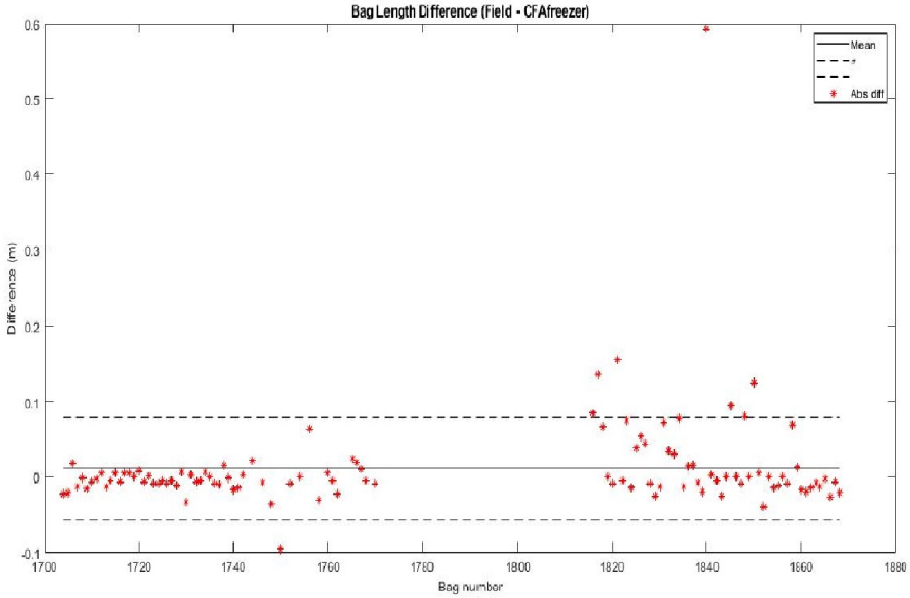


**Figure 20:** *Bag length offsets between field measurements and CFA freezer measurements*

Since this error accumulates with depth, it proved to be a significant source of error in correct depth and thereby, age assignments of the data. Therefore, it was decided that the start depth of each bag should be constrained to the actual field logged depth. Figure 21 shows this correction made to the data for Run 1738. An offset of 0.1310 m was calculated for this particular run of 9 bags, implying an uncertainty in age assignment on a decadal scale.

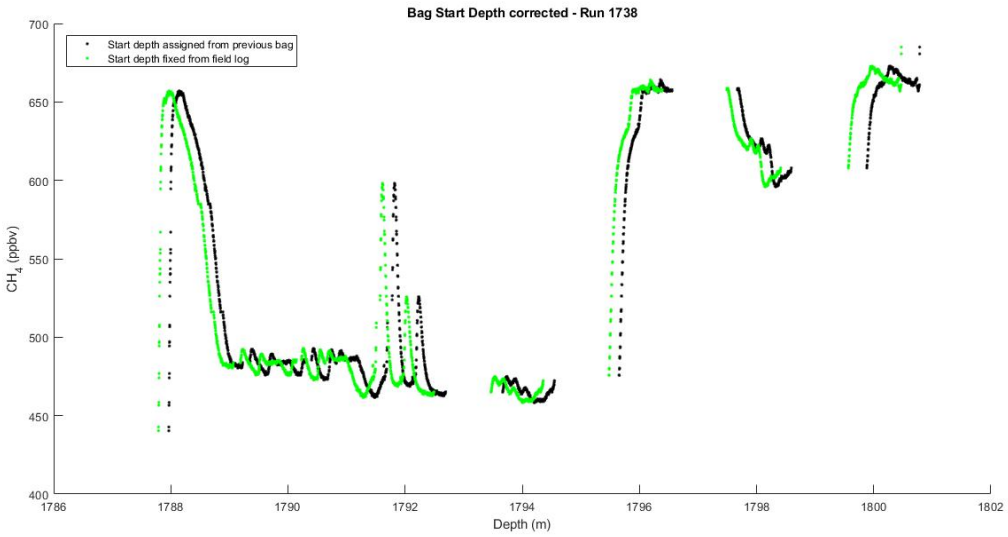


**Figure 21:** *$CH_4$ vs Depth with start depth of each bag assigned to be the field logged start depth*

As previously mentioned, most of the bags seemed to be longer than the field measurements. This meant that by assigning a fixed start depth, there would be an overlap of data. Hence, the calculated end depth of each bag was compared to the expected end depth from the field measurements. If the calculated depth was shorter, no changes were made. However, if the calculated depth was longer, all the data for the bag after the point of minimum difference were negated. Figure 22 shows this correction and Figure 23 shows the final $CH_4$ vs Depth data for this run, with contamination spikes removed.

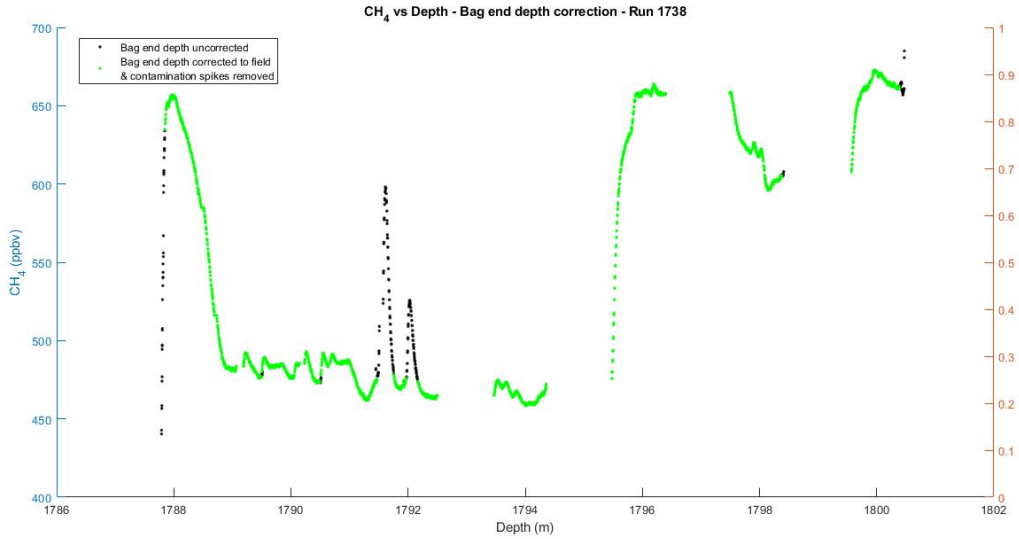


**Figure 22:** *$CH_4$ vs Depth with bag end depth corrected to match field log; data removed where too long. Contamination spikes have been removed.*

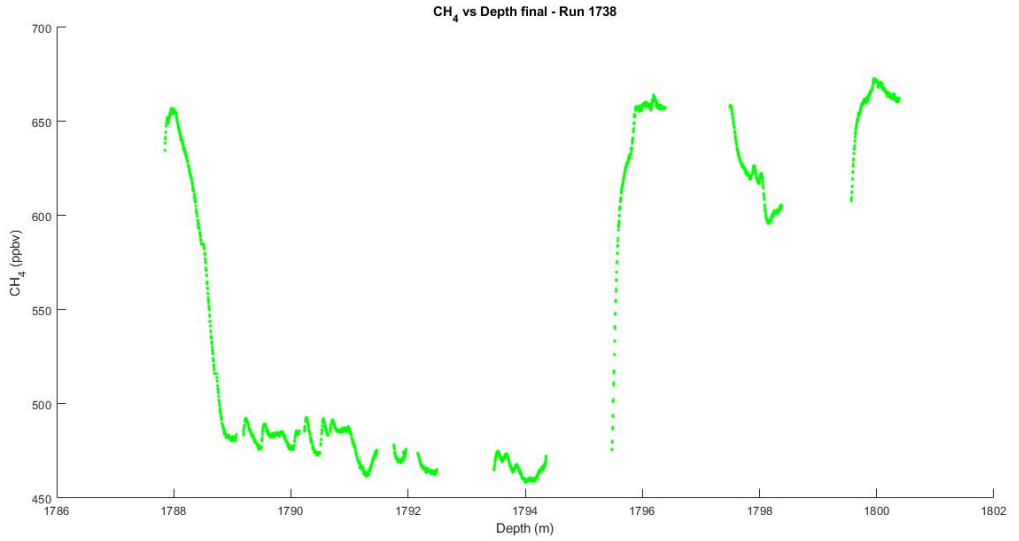


**Figure 23:** *Final $CH_4$ vs Depth with corrections made to the raw data, showing the Younger Dryas transition and the transitions into Bølling-Allerød.*

# 4 Discussion

## 4.1 System Uncertainties

All the calibration tests for the module were done at a constant temperature of 30°C. Tests had been performed initially to determine the effect of temperature on the extraction efficiency of the module; however, it was later found that the there was a crack in the outer casing of the module which was introducing leaks. Since it was uncertain whether the leak had existed during the temperature tests, those results had to be discarded and could not be repeated due to paucity of time. Nevertheless, data from an as yet unpublished work by a colleague *(Jesper Baldtzer Liisberg, personal communication, 2020)*, shows that there are temperature effects on the gas extraction, which are more pronounced at higher mixing ratios of $CH_4$. Assuming 100% equilibrium between gas and liquid at the micromodule, Henry's law constants for $N_2$, $O_2$, Ar, and $CH_4$ were theoretically estimated in the range of temperatures and pressures observed during the campaign, taking into account the liquid to gas flow ratio. From this estimation, it can be deduced that varying temperatures shift the degree of solubility of the different gases. Figure 24 shows the difference between the resulting expected offset in mixing ratios of methane measured at varying temperatures, assuming the baseline to be the mixing ratio at 22°C, which was the average ambient temperature in the laboratory. Considering the range of temperatures in the laboratory recorded during the campaign, even at 100% equilibrium, the offset between Glacial and Holocene levels is not more than 1 ppb, and the maximum offset not more than 3 ppb (Figure 24).

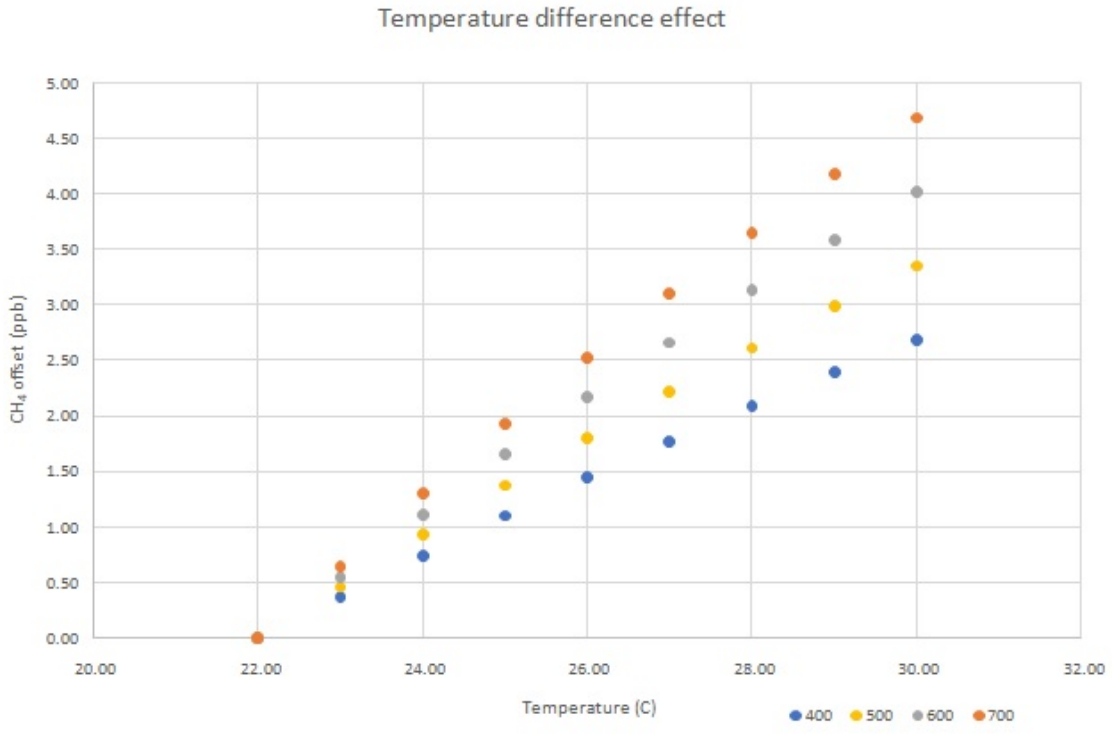


**Figure 24:** *Temperature effects on measured $CH_4$ mixing ratios from 22°C to 30°C, assuming 100% equilibrium at the micromodule. (Courtesy: Jesper Baldtzer Liisberg)*

This effect of temperature is yet to be fully quantified, but since all measurements were done at room temperature, with a record of the daily temperature maintained, it might be possible to correct for these effects based on the data of temperature and flow. The range of this correction

is not expected to be more than ± 3 ppbv, given the ambient temperature range in the CFA lab during measurements. Moreover, the maximum shellside working liquid temperature for the module is designed to be in the range of 5-25°C (*3M, Liqui-Cel MM-0.75X1 Series Membrane Contactor*) which would ultimately limit the temperature control possible, though the sample stream itself does fall into that range. It would however, behoove future campaigns and data processing to repeat temperature experiments on the module to rightly establish the effect it has on the extraction and on module lifetime.

In the final set-up for this measurement campaign nonetheless, it was ultimately decided to discard the temperature control of the extraction box in favour of accessibility to the module and surrounding tubing. It was found that due to the less than optimal tubing connection that had to be made because of the strange shell dimensions of the module, it was imperative to reduce kinks in the lines as much as possible. The orientation of the module and the proximity of the 1/8" tubing to the membrane interface was imperative to uninterrupted flow. On more than one occasion, the tubing or the connections had to be carefully nudged to prevent gas bubbles from sticking to the tubes at restrictions. Since this was the first time the micromodule was implemented in the CFA system as the main gas extraction unit, the overall lifetime of the module in the continuous system was unknown. It was decided to replace the module after 4 weeks of melting owing to infrequent, yet significant intermittent drops in gas flow. This may, in part, be explained by the fact that the module was not permeable to dust particles.

A test experiment was conducted on less dusty Holocene ice from the Mount Brown South ice core, by bypassing the filter before the micromodule and connecting a second Abakus laser sensor (Klotz, Abakus Particle counter for fluids) to the chemistry sample stream from the micromodule's liquid outlet, in addition to the Abakus laser sensor measuring the particles on the dust sample line extracted from the debubbler. It was discovered that the micromodule filtered particles of size >= 8 µm. A distinct difference in particle counts was also observed between the two Abakus instruments, a clear indication that the membrane was being clogged by particles. Despite using a 20µm filter, since most of the ice melted during the Dye-3 campaign were from dusty glacial sections, it is possible that the module was exceptionally quick to deteriorate.

An additional indicator of declining module efficiency could be that bubble accumulation was observed at the interface of the 1/8" HPFA tubing and the membrane array, which increased in frequency over time. It appeared as though the gas extraction decreased until the pressure at the membrane interface built up enough to provide a sudden surge of gas flow. In future CFA campaigns, it would be prudent to replace the module after a maximum of 2 weeks (perhaps earlier in case of continuous exposure to large dust particles as would be indicated by a drop in the liquid flow), and also attempt to place the membrane array in a different shell that supports connections for regular tubing dimensions.

Additionally, all calibration tests for calculating the extraction efficiency of the module were done with $N_2$ gas in place of a $CH_4$ standard. $N_2$ has a lower solubility of ($6.4 \cdot 10^{-6}$ $\frac{mol}{m^3 Pa}$) in $H_2O$ as compared to $CH_4$ ($1.4 \cdot 10^{-5}$ $\frac{mol}{m^3 Pa}$) at STP (Sander, 2015) which would have a small impact on the results obtained. The path length of the calibration set-up was also significantly shorter, with lesser restrictions, than the final set-up. Also, as previously mentioned, since it was not possible to pull the segmented flow of mQ water+gas through the pump owing to the dead volumes along the path, it became necessary to independently set the pump speed for the liquid and the MFC for the gas to obtain a total combined flow of the desired value. However, the measured flow was not as expected, with the liquid flow always slightly lower than set to,

affecting the real total flow and the actual gas percentage (see Appendix 1). This implies that the calculated extraction efficiency of the module does not sufficiently account for dissolution along the path and restrictions in the system, and is therefore overestimated by a small magnitude. However, it must also be noted that the tests for the total expected flow at 18, 20, and 25 ml/min were done on the same day, while the tests for the flow at 23 ml/min was done the next day. This meant that conditions were slightly different in terms of new mQ water and new pump tubing, both of which can slightly affect the results, though not significantly.

Flow effects on the whole system were initially assumed to be leaks but the final set-up was spiked with a 5% $CH_4$ mixture and was confirmed leak tight. Tests done on the leak tight system with dry gas (the results of which are shown in **Section 3.2**), confirmed that the Picarro overestimated mixing ratios at lower flow rates. The reason for this is as yet unexplained, but can be corrected for as previously elaborated. On the other hand, it is hard to account for instrumental drift based on calibration runs through the course of a day, and through the duration of the campaign. This is due to the fact that all calibration runs were done by passing a mixture of mQ + standard gas through the system, with the mQ water being supplied from a 5 L bottle continually degassed with $N_2$ at 60 ml/min (from the combined outflow of the two Nafion purge streams). The bottle was filled to a different level each time and degassed for slightly different amount of time each time as well. Therefore, values recorded were consistently lower than the dry gas measurements; however, small variations were observed each time, owing to a combination of $N_2$ saturation in the mQ water and dissolution in the system. The impact on calibration measurements of a non-standardized protocol for degassing the mQ water was not immediately identified, making it difficult to estimate the true values of $CH_4$ mixing ratio in 100% degassed mQ water for this set-up. Thus, the calibration data have not been used to correct for dissolution and drift in measurements.

### 4.2 Depth Scale

The depth calculation from the encoder data was found to be highly dependent on the chosen threshold values. Typically, the encoder counts dropped to 0 as it was brought down level with the melthead during a frame change. However, at the end of the run, when 2 blocks of 3.5 $\times$ 3.5 cm mQ ice were added for calibration purposes, it was not necessary to remove the whole frame and therefore, the encoder was not brought down all the way to a 0 value. The difficulty this posed during data processing was when a common threshold value had to be chosen for deciding indices to interpolate across in the calculated melt rate data (Figure 26). Due to the last 'frame change' interval, which is the addition of the mQ block, it was not possible to choose a threshold value lower than the encoder value during that change (Figure 25). Based on depth calculations for all the runs, the best agreements of interpolated to measured values were, in fact, obtained for runs where the data had to be manually screened for every frame change due to the encoder breaking down, allowing the opportunity to minimize interpolation intervals for each frame change independently. However, for multiple runs with 9 or 10 bags each, this would be a laborious and tedious process, and can be avoided by ensuring that the encoder is always brought down to 0 counts when adding the mQ ice.

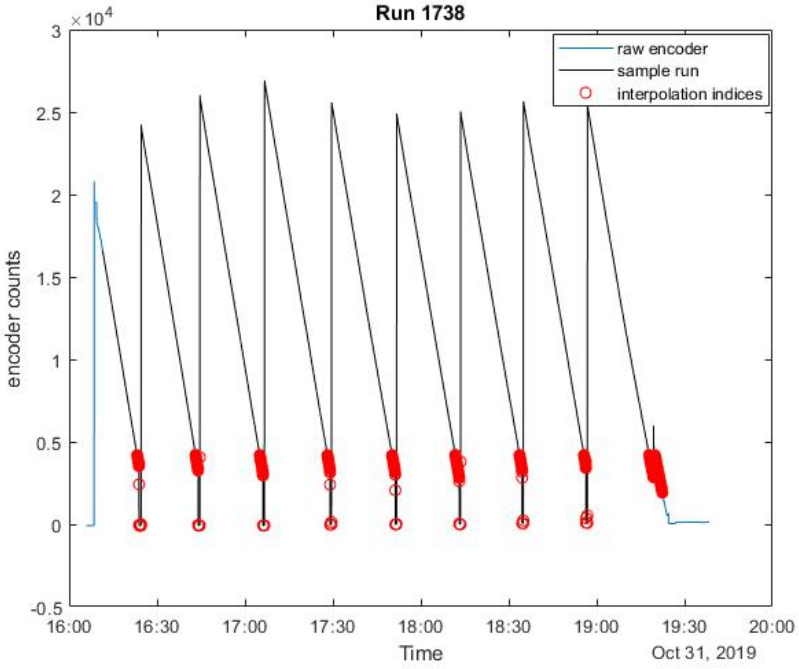


**Figure 25:** *Example of indices chosen for interpolation based on the encoder data - Run 1738*

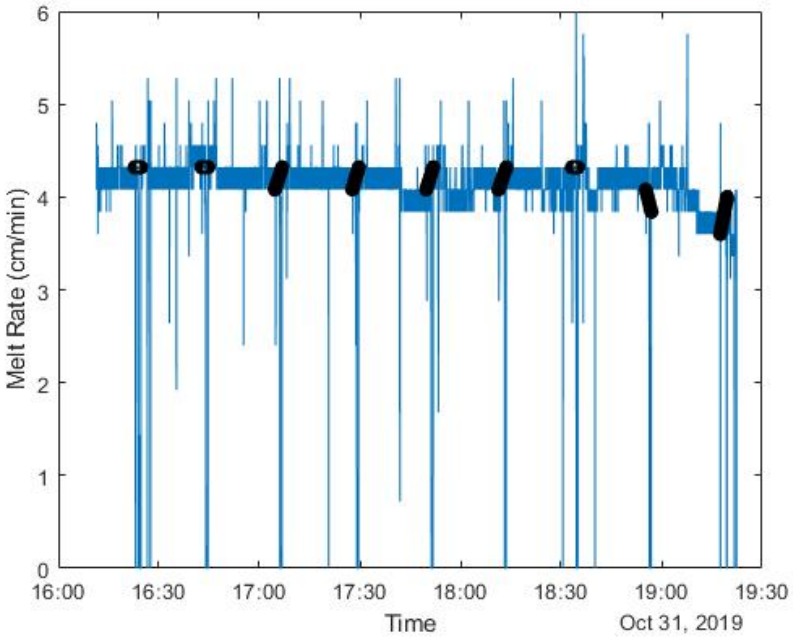


**Figure 26:** *Example of interpolation indices chosen for the melt rate data based on the encoder threshold - Run 1738*

Nevertheless, it must be noted that in some cases, it was quite difficult to get a calculated value close to the measured length. One such case is shown in Figure 27, where the melt rate values derived from the encoder counts appears extremely noisy for bag 1832. In this particular instance, it was due to the ice being 1 mm too wide along all edges; hence, the ice stick was stuck to the sides of the frame and manually guiding it down to the melthead proved to be a finicky process for the encoder counts to maintain a smooth slope as is desired.

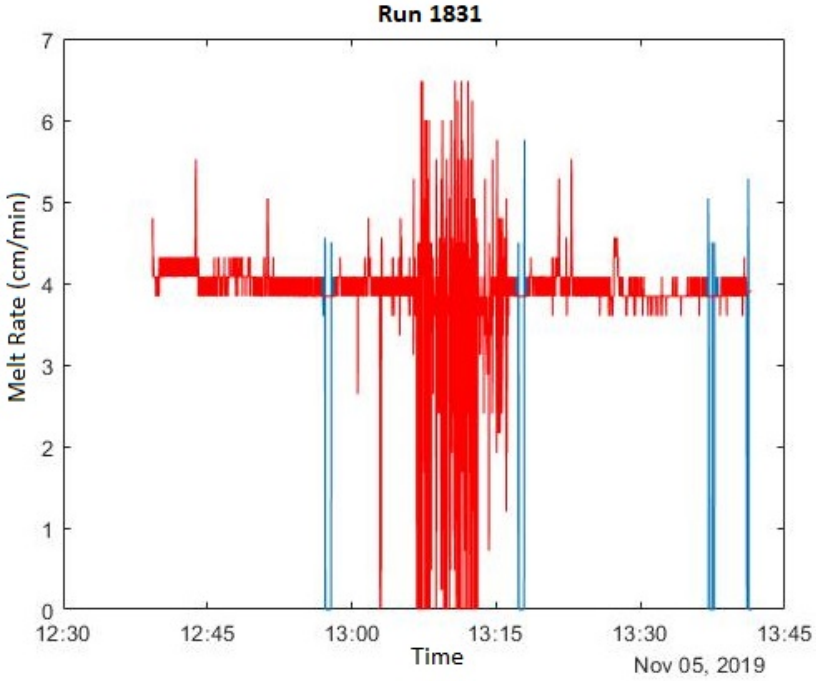


**Figure 27:** *Example of melt rate calculated from encoder data for a finicky bag of ice - Run 1831*

Uncertainties in depths were first noted not by comparison with field logs, but actually because there were strange and significant outliers between the calculated depth and the CFA freezer measurements, especially in some cases where the calculated depth was longer. Upon rechecking the cutting logs, discrepancies were found due to inconsistencies in protocol for recording measurements, between the multiple people involved in the cutting. With this particular campaign, it proved to be instrumental in noting the much bigger uncertainties presented by the ice itself; however, in future campaigns where the total depth of ice measured is potentially a lot more, it would be imperative to have a standardized operating protocol for various aspects of the CFA campaign, from records in cutting logs, to degassing mQ water for standard runs, to improved logging during the melting runs.

A case in point of the importance of laboratory logs is the alignment of contamination spikes on the depth scale for this particular core. Since the gas flow varied significantly from bag to bag, affecting the delay times, the most straightforward method to verify the calculated delays was to check whether contamination spikes lines up with recorded breaks in ice during melting. However, such a check can inadvertently lead to a confirmation bias since it is not necessary that contamination spikes in data always correspond to a break and vice-versa. Especially in the case of an old ice core such as Dye-3, it is possible that contamination has occurred due to handling over the years or, from refrozen breaks that were not noted while melting. Fortunately, a few such spikes were made note of during the laboratory logging, which brought other possibilities into consideration and prevented a bias in processing.

A second check was made possible by the fact that $N_2$ and Ar isotopes were measured in parallel by a mass spectrometer. The delay time to the Picarro was calculated as a sum of the delay from the melthead to the micromodule, and the delay from the micromodule to the Picarro. However, since the sample to the mass spectrometer was extracted right after the micromodule, at a constant flow using a capillary, the delay to that system is quite constant. Therefore, aligning the data from the two instruments gave a second verification of the calculated

delay times to the Picarro (Figure 28).

A third, further confirmation of the assigned depth scale with calculated delays can be made in the future by confirming with the conductivity data from the wet chemistry measurements, that contamination spikes line up where expected from the $CH_4$ data, so as to ultimately have a common depth scale for all the measurements made during the campaign. This would be important for further determination of $\Delta$age between the ice and gas.

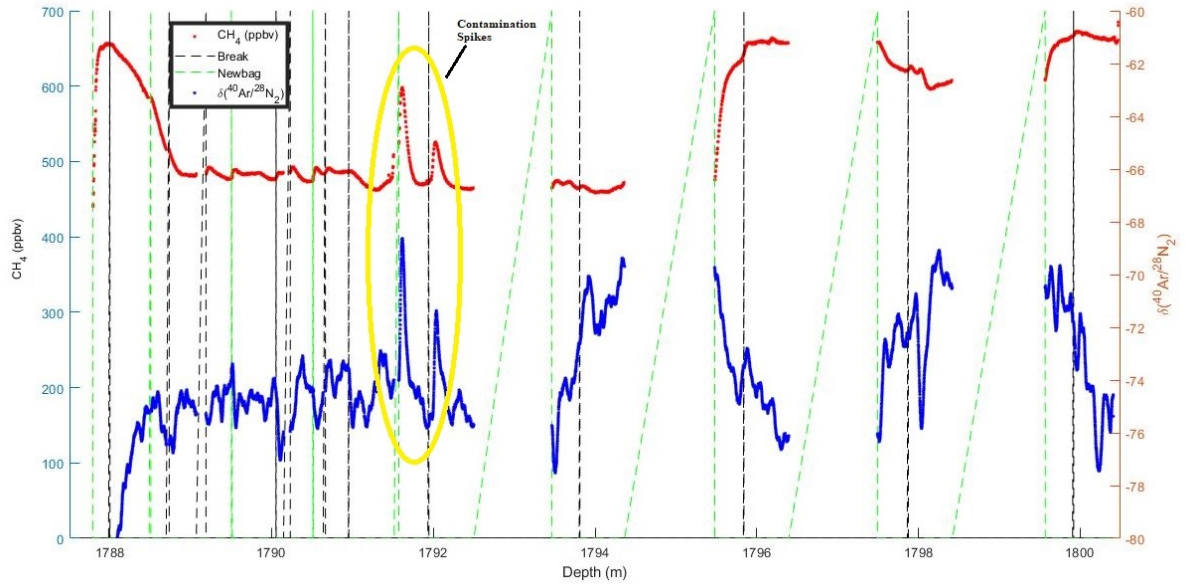


**Figure 28:** *$CH_4$ and $\delta(\frac{^{40}Ar}{^{28}N_2})$ plotted on a depth scale for the section of ice under analysis. Contamination spikes (marked by the yellow circle) line up at depths where breaks in the ice were logged. Spikes in the two data sets are also aligned, verifying the estimated delay times.*

In terms of offsets in recent measurements compared to the field logs 40 years ago, it would be interesting and also important for further data processing, to verify the amount of thinning in the deeper sections of the core. Considering that the accumulation at Dye-3 during the last glacial was only 0.142 m/yr ice equivalent (Supplementary Information, Vinther et al., 2009), the thinning of the ice in deeper sections, in conjunction with accumulated offsets in measured depth, may affect the age assignment of the deeper ice on the order of decades to centuries, perhaps more. As for the section under analysis, *Rasmussen et al., 2006* estimated the duration of the Younger Dryas to be 1193±39 years from a common stratigraphic timescale developed for the NGRIP and GRIP ice cores. Arbitrarily estimating the depth interval of this duration to be 6 m in the Dye-3 core based on preliminary observations in the data, the average annual layer thickness in the core during this period was calculated to be 0.005 m. Therefore, an accumulated depth error 0.1310 m can equate an age uncertainty on a decadal scale. By constraining the bag start depth for each bag, and negating data beyond the expected end depth of each bag based on field logs, the errors have been limited to individual bags and prevented from accumulating with depth. Accounting for these errors however, would bring more clarity to the dataset.

### 4.3 Data Analysis

Monitoring the flows of liquid and gas at all points of extraction allowed for the possibility of estimating the gas percentage in the sample, as described in **Section 3.1**. Figure 18b shows the gas percentages as bag means for the section of ice under analysis. It can be observed that the total air content in the sample, expressed as the gas% is at most 7% and mostly lower, in the 9 bags encompassing this particular melting run. Upon consulting previous measurements on total air content in the Dye-3 ice core, it was found that different sources measuring at different time periods since the ice was drilled, found similar results. *Craig and Chou, 1982* found the mean air content to be 93.8±7.3 cc(STP)/kg upon measuring at 16 depths along the core length, while analysis of a section with a visible melt layer at Bern (Supplementary Information, Vinther et al., 2009) showed similar values with an expected drop only at the melt layer, where solubility was assumed to be the main driver affecting the gas concentration (Figure 29).

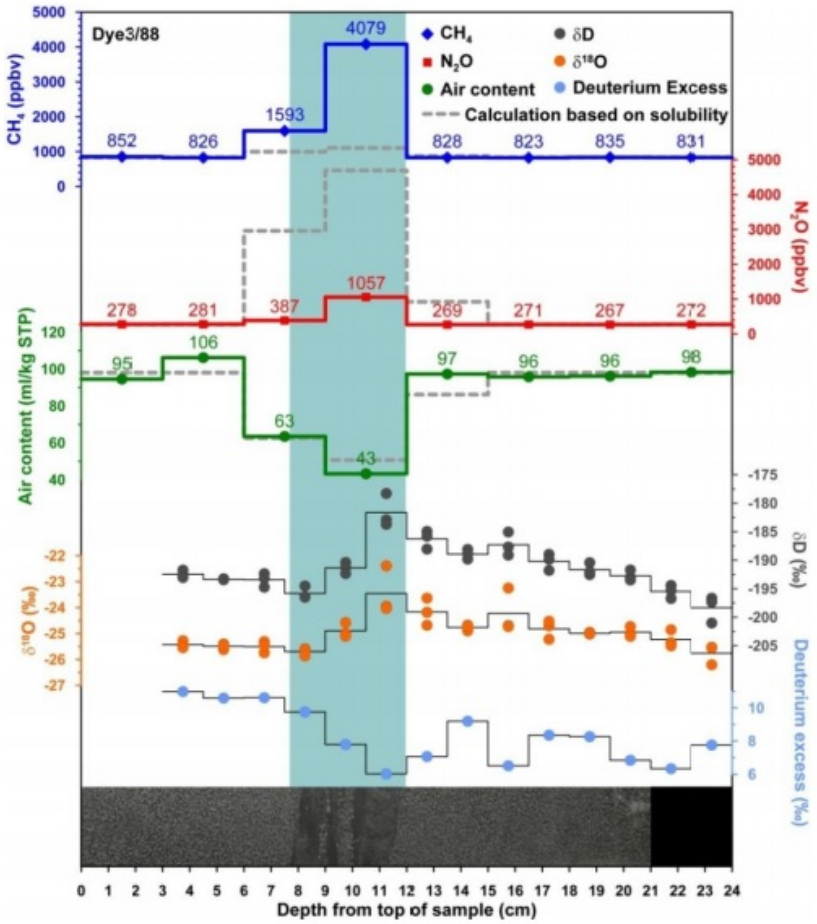


**Figure 29:** *Caption from source: 'Analysis of a clearly visible melt layer in ice from Dye3 at a depth of 88 m. At the University of Bern, consecutive samples of 3 cm length are measured for $CH_4$, $N_2O$, and air content and consecutive samples of 1.5 cm length are measured for $\delta D$ and $\delta^{18}O$ ice, from where deuterium excess is calculated. The melt layer is indicated by the blue shading and the picture of the ice sample at the bottom of the plot. The dashed grey lines show the expected values for $CH_4$, $N_2O$, and air content under the assumption that solubility is the only mechanism affecting the gas concentrations in the melt layer' (Source: Supplementary Information, Vinther et al., 2009).*

While melt layers may be an explanation for exceptionally low gas percentages measured in this campaign, they do not explain the consistently lower-than-expected mean that is observed. Although the data from the remaining sections of ice are yet to be processed, it can already

be said from real-time observations during the campaign that the gas content with respect to the liquid flow was persistently less than the expected 10% of sample. Since all the flows in the sample line are measured and accounted for, one theory could be that the melthead peristaltic pump was simply not performing to the expected efficiency due to restrictions along the flow line and therefore, an excess of gas was pushed to the outer waste lines. Additional flow meters monitoring the flows in the outer lines could, perhaps, account for this loss of gas.

The other effect of varying gas flow lies in defining the depth resolution of the measurements. While the Picarro analyser has an effective volume of 0.57 ml at 45 Torr, the micromodule has an effective shellside volume of 1.92 ml at a gas pressure of 300 mbar, calculated as,

$$V_{eff} = V \cdot \frac{p_{op}}{p_{std}} \tag{7}$$

$V_{eff}$ = Effective shellside volume at 300 mbar

V = Shellside volume at STP (6.5 ml, 3M, Liqui-Cel MM-0.75X1 Series Membrane Contactor)

$p_{op}$ = Operating pressure on the gas side (300 mbar)

$p_{std}$ = Pressure at STP (1013 mbar)

Given the average melt rate of 4 cm/min, the depth resolution can vary between 4 cm to 8 cm for gas flows ranging from 1-2 ml/min.

For further analysis of the robustness of the data, a comparison plot was made for the Younger Dryas section measured in this campaign, against discrete $CH_4$ data from NGRIP (Baumgartner et al., 2014), GRIP (Chappellaz et al., 2013), GISP2 (Chappellaz et al., 2013) (Figure 30). All 3 reference ice cores cover a section spanning in age from ca. 11.4 kya to 13.3 kya, starting in the early Holocene, transitioning into the Younger Dryas and covering the beginning of the Bølling-Allerød interstadial. However, the $CH_4$ values measured here from Dye-3 are consistently lower than the values recorded in the other ice cores representing a wide spatial coverage of the Greenland Ice Sheet. The Holocene values are on average 50-80 ppbv lower than the other cores, and the stadial values 20-30 ppbv lower. These values are outside the range of uncertainties for all the different measurements from the different ice cores compared with. The absolute measurement of the one discrete data point for Dye-3 in this depth range from *Stauffer et al., 1988* agrees within the uncertainty for the 2019 measurement at that depth. However, upon adding the uncertainty for the 1988 measurement, it again falls in the bracket of the $CH_4$ (ppbv) range from the other ice cores. Therefore, it hard to discern the agreement between the datasets. Newer discrete measurements along sections of the core would provide a better context to the lower values observed in the continuous measurements.

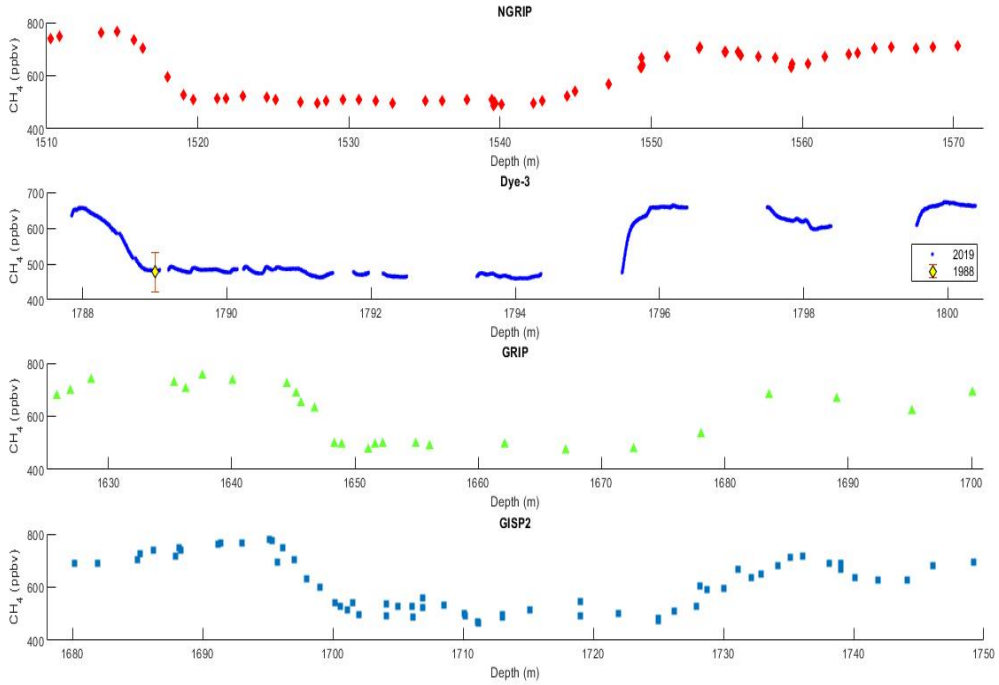


**Figure 30:** *Comparison of current Dye-3 measurements against discrete $CH_4$ measurements (ppbv) NGRIP (Baumgartner et al., 2014), GRIP (Chappellaz et al., 2013) and GISP2 (Chappellaz et al., 2013) for the Younger Dryas section, plotted on the individual depth scales. One discrete $CH_4$ measurement from Dye-3 for the section under analyses, is also plotted for comparison of values (Stauffer et al., 1988).*

*Landais et al., 2013* observed a preferential loss of 3 - 8% $O_2$ from the Vostok ice core, which affected the $\delta^{18}O$ measurements, but no corresponding discrepancies between the new and old Vostok methane measurements were observed, indicating little to no loss of $CH_4$ during storage. A recent study by *Lee et al., 2020* found excess $CH_4$ in discrete measurements of dusty glacial ice following a method of melt extraction. The anomalies measured were on the order of 30-40 ppb methane and comparable in the NGRIP, GRIP and GISP2 records. Such anomalies are not observed in continuous measurements where there is little time of interaction between the meltwater and the gas bubbles, before the gas is extracted (Lee et al., 2020). *Hammer et al., 1985* found that the dust concentration in the Younger Dryas measured in the Dye-3 ice core was only around 0.5 mg/kg as compared to 1.84 mg/kg in GRIP (Svensson et al., 2000) and 1 mg/kg in NGRIP (Ruth et al., 2003). Notwithstanding the fact that the source and composition of the dust particles would also play a role in causing this observed methane excess, Figure 30 has been made as a comparison with these same cores that *Lee et al., 2020* found anomalies in, and the range of the difference in the stadial values of the Dye-3 record from the other cores, is comparable to the range of excess methane observed in Glacial periods in these cores by *Lee et al., 2020*. However, this observed $CH_4$ excess is specific to dusty glacial periods. It still does not explain the offsets in the interstadial values, which are approximately double the stadial levels, proportional to difference in the $CH_4$ mixing ratios between these climatic periods.

Therefore, the problem may be isolated to the extraction system. Instrumental calibration offset corrections (**Section 3.2**) confirmed that corrected values from the dry gas measurements agree with the real values of the $CH_4$ mixing ratios in the two standards. Moreover, all the materials used in the system have remained the same over the years and there is no known part

that might consume methane upon interaction. Thus, further constraining the problem to the path from the melthead to the micromodule, the only components are the pump, the Melthead valve, the debubbler for dust sample extraction, the particle filter, and the Bypass valve, along with the 1/8" HPFA tubing and the liquid water that the gas bubbles interact with.

Given the speed of melting and the shorter path length, it is not expected that equilibrium would be reached between the gas phase and the liquid phase before reaching the micromodule. Therefore, solubility of $CH_4$ in water cannot explain the magnitude of deviation from expected values based on other records. There are no visible gas bubbles lost to the dust sample line; therefore, the arbitrary assumption that 10% of the dust line is gas used in the total gas measurements in this work is actually a significant overestimation leading to the conclusion that gas loss at the debubbler can also not explain the difference in $CH_4$ magnitudes observed between the different datasets. The particle filter used had a pore size of 20 µm and is thus too large to selectively block methane molecules, which have an effective diameter and effective length of 3.988 Å (Mao and Sinnott, 2001). Although the calibration values have not been used to correct the dataset since the degree of $N_2$ saturation in the mQ water remains unknown, the values were always, on average, 660±10 ppbv for the Holocene standard and 385±5 ppbv for the Glacial standard. Comparing to the uncorrected dry gas measurement values from the WS-CRDS of the two standards - 684.21±0.21 ppbv and 386.58±0.31 ppbv respectively, it is a further indication that solubility is not the main explanation for this magnitude of difference in measurements from the present set-up. Therefore, the only conclusion derived at present is the fact that there is no clear explanation based on the current observations and understanding of the set-up. Further experiments are needed to characterize the individual components of the set-up, perhaps also in addition with more current discrete measurements from this core, before any conclusions may be drawn. It also remains to be confirmed from further data processing, whether this systematic error in measurements, that appears proportional to the mixing ratio, is persistent through all the sections of ice measured.

## 4.4 Summary of system changes

I. **Improvements from older set-ups**

- Multiple flow loops have been eliminated and the whole system has been compacted to one sample flow loop with lesser components, allowing for faster travel time and less time for liquid dissolution in the system
- The common debubbler-micromodule tandem from previous set-ups (e.g., Chappellaz et al., 2013) have been replaced by a single micromodule of higher flow capacity, leading to lesser dead volume and higher extraction efficiency
- It was found during the set-up phase that a less restrictive tubing dimension for all liquid flows (1/8" HPFA in this case), made a significant impact on measured liquid flows in the sample line, which were previously on the order of 10 ml/min lower than the melthead peristaltic pump setting
- A faster melt rate of 4 cm/min as compared to previous campaigns with 3 cm/min, coupled with operating at a lower cavity pressure of 45 Torr lead to higher data quality due to a faster renewal rate of the cavity, and lesser time for dissolution in the liquid phase
- Running a standard with low concentration of $CH_4$ before the run has a dilution effect that minimizes contamination from mQ ice at the beginning of each run. Longer runs of around 9 bags per run also minimized this data loss
- In earlier set-ups, the pressure gradient across the extraction module, which is the main driver for extraction, was regulated solely by the inlet valve of the Picarro, reaching only a $\Delta P = 300$ mbar. Using a back pressure regulator, it is now regulated to 700 mbar which facilitates higher extraction across the membrane module
- Monitoring the pressure and flow parameters at every point of separation along the system enables an estimation of total air content in the sample stream which has not been measured previously. However, the values are not precise enough to see small changes in air content related to climate changes. The measurements can rather be used diagnostically
- Parallel gas measurements allow for a cross-verification of calculated delay times to the instruments based on flow
- Effects of low flows of Picarro measurements were observed and incorporated into corrections for instrumental calibration offset

II. **Future scope**

- A dedicated gas-only CFA set-up decoupled from the wet chemistry would allow for reducing the number of valves, connections and restrictions through the whole system, giving better flow conditions
- A 1-2 cm extra ice removed at misaligned ice or breaks with higher probability of contamination can reduce the intrusion of ambient air. This can prevent 5 minutes of data loss while the Picarro re-stabilizes which, when melting at 4 cm/min, would amount to 20 cm of data lost. In deeper sections of the core, this can mean hundreds to thousands of years
- Although in this particular campaign, temperature control of the extraction unit was neglected in favour of accessibility to components, it would overall be better to have a constant temperature around the point of extraction as it would have an impact on extraction efficiency and ease data processing
- Standardized protocol for degassing mQ water for calibrations before and after runs is imperative for correcting for drift in measurements
- Degassed mQ water for making the mQ ice preceding each sample run to flush the lines would prevent contamination spikes from the mQ ice and prevent data loss in the beginning of each run
- Measuring the gas flows in the outer waste lines may explain the lower-than-expected gas% measured in the sample line
- Standardized protocol for cutting logs and laboratory logs for improved data quality and more precise depth assignment
- Encasing the micromodule in a different shell compatible with regular tubing connections would prevent bubble accumulation at the membrane interface and reduce sample mixing in the small dead volume therein
- Module extraction efficiency calibrations must be redone in the future in the final set-up, with multiple standard gases so as to better characterize the effects of dissolution, equilibrium, and methane mixing ratio on the extraction
- Although emperical evidence showed the effect of low flow on WS-CRDS measurements, the cause is still unknown and needs to be further investigated

# 5 Conclusions

Improvements were made to the existing gas-CFA system in an effort to affirm data quality. The system was simplified to incorporate a shorter path length, lesser dead volumes, and a faster speed of melting. A single membrane module was used as the main extraction unit and an optimal constant pressure gradient was maintained between the liquid and gas phases, in order to reduce solubility effects and increase extraction efficiency. The effective volume of the micromodule under the operating conditions was calculated to be 1.92 ml. At the average melt rate of 4 cm/min of ice, this leads to a depth resolution of 4-8 cm at the micromodule at the observed gas flow rates ranging between 1-2 ml/min. The calibration offset at the lower operating cavity pressure at the Picarro analyzer, and the measurement error caused by varying flows were corrected for every data point as a function of the measured $CH_4$ mixing ratio and the gas flow rate to the Picarro. The mean correction factor for the section of ice under analysis was found to be 13.05±1.36 ppbv. Adding the uncertainty from temperature and solubility effects, the total uncertainty of measurements is expected to be around ±5 ppbv. A depth scale was assigned to the $CH_4$ data and offsets were noted between the measured bag lengths and the field logged depths. These errors were constrained to individual bags by assigning the start and end depths of each measured bag to the logged depths. The average annual layer thickness in the Dye-3 ice core during the Younger Dryas is about 5 mm. This implies an age resolution on a decadal scale, corresponding to the estimated depth resolution of the data. The Dye-3 $CH_4$ record for the Younger Dryas section was compared to discrete measurements of this period from the NGRIP, GRIP, and GISP2 ice cores. The corrected $CH_4$ data from the present Dye-3 measurements proved to be systematically lower than the $CH_4$ record in the other ice cores, well beyond the estimated uncertainty of measurements. Some theories have been explored to explain this offset; however, further investigation is needed before any conclusions can be drawn. Additionally, potential upgrades to the system have been identified based on this work and suggestions made to improve data quality.

# 6 Acknowledgements

This work would not have been possible without support and guidance from a number of people in different ways and who must be acknowledged here.

First and foremost, I would like to thank my supervisor, Thomas Blunier, for his infinite patience, support, and encouragement, and for his constant guidance even while allowing me the freedom to experiment, explore and shape this work to my interest as I went along.

I must thank Jesper Baldtzer Liisberg for being a reassuring presence in the lab, and for uncomplainingly being the go-to person, be it for troubleshooting instruments, or for troubleshooting life on bad weather days.

I would be remiss in my duty if I did not thank my Head of Studies, Anders Svensson, for his constant good humour and encouragement, and for having my back as I completely tailored the MSc Climate Change program according to my specific interests.

CFA campaigns are always fun, despite long hours and stressful situations, and it is the people that make them so. The Dye-3 CFA campaign would not have been the same without Thomas Blunier, Paul Vallelonga, Helle Kjaer, Anders Svensson, Todd Sowers, Andy Menking, Rachael Rhodes, Jesper Liisberg, David Soestmeyer, Lara Moellney, Jia Mei-Lin, Meg Harlan, Aylin de Campo, Anna Klüssendorf and Zurine Yoldi. Thank you for company on the everyday shifts, the celebrations, the cake, and constant good humour in the lab!

Speaking of labs, my time working in the Gas Lab at PICE this past year would not have been the same without Jesper, Elena, Lara, David, Maureen, and Amal, who have made this a very memorable time in my life.

Estelle, Mathias, and Pernille pulled me into their physics group and became such dear friends, as I tagged along on all the geophysics courses I could take these last two years. My masters would not have been the same without them. And I'm especially glad I got to share my first field experience at EGRIP last year with Estelle.

I must also give a very special thanks to Iben for all the late night company these last two years; and equally special thanks to Eliza, Tamara, Giulia, Julien, Lisa, Tyler, Rici, Caroline, Sainath, Roopa, and Shruthi, for their kindness, and constant and unflinching emotional support that enabled me to focus on my thesis even through rough patches.

Nancy Bertler is one of the kindest people I know, who gave me my first CFA experience and introduced me to the world of ice core science, which has led me to where I am today and I am forever grateful to her for that experience.

Two very special people I must thank are Dhee, who keeps me grounded - something I need very often, and Grinch with a heart two sizes too big, who taught me patience, determination and perseverance - the things that kept me pushing the extra mile.

Last but not the least, I must thank my family for their rock-solid belief in me in all my endeavours over the years, and without whose support I would not have been able to move to Copenhagen to pursue this masters as I dreamed of doing. And finally, this is for my dad.

# References


[1] 3M. *3M, Liqui-Cel MM-0.75X1 Series Membrane Contactor*. URL: https://multimedia.3m.com/mws/media/1412487O/3m-liqui-cel-mm-0-75x1-series-membrane-contactorlc-1006-pdf.pdf. Accessed on 21/01/2020.

[2] National Oceanic & Atmospheric Admisnistration. *Global Distribution of Atmospheric Methane, NOAA ESRL Carbon Cycle*. Accessed on 18/01/2020.

[3] M Baumgartner et al. "NGRIP CH4 concentration from 120 to 10 kyr before present and its relation to a delta15N temperature reconstruction from the same ice core". In: *Climate of the Past* 10 (2014).

[4] Matthias Bigler et al. "Optimization of High-Resolution Continuous Flow Analysis for Transient Climate Signals in Ice Cores". In: *Environ. Sci. Technol.* 45 (10 2011), pp. 4483–4489.

[5] T Blunier and E J Brook. "Timing of Millennial-Scale Climate Change in Antarctica and Greenland During the Last Glacial Period". In: *Science* 291 (109 2001), pp. 109 –112.

[6] E J Brook. "Ice Core Methods: Overview". In: Encylopaedia of Quaternary Science 2nd Ed., Elsevier, 2007, pp. 1144 –1154.

[7] Julien Browaeys. "Linear fit with both uncertainties in x and in y". In: *MATLAB Central File Exchange* (2020). https://www.mathworks.com/matlabcentral/fileexchange/45711-linear-fit-with-both-uncertainties-in-x-and-in-y. Retrieved January 18, 2020.

[8] J Chappellaz. "Ice Core Methods: Methane Studies". In: Encylopaedia of Quaternary Science 2nd Ed., Elsevier, 2007, pp. 1199 –1206.

[9] J Chappellaz et al. "High-resolution glacial and deglacial record of atmospheric methane by continuous-flow and laser spectrometer analysis along the NEEM ice core". In: *Climate of the Past* 9 (2013), pp. 2579–2593.

[10] CIC. *CIC, Densification*. URL: http://www.iceandclimate.nbi.ku.dk/research/flowofice/densification/. Accessed on 03/01/2020.

[11] CIC. *CIC, Drilling to Bedrock*. URL: http://www.iceandclimate.nbi.ku.dk/research/drill_analysing/history_drilling/drill_bedrock/. Accessed on 31/12/2019.

[12] CIC. *CIC, The firn zone: Transforming snow to ice*. URL: http://www.iceandclimate.nbi.ku.dk/research/drill_analysing/cutting_and_analysing_ice_cores/analysing_gasses/firn_zone/. Accessed on 03/01/2020.

[13] H Craig and C C Chou. "METHANE: THE RECORD IN POLAR ICE CORES". In: *Geophysical Research Letters* 9 (11 1982), pp. 1221–1224.

[14] A Dällenbach et al. "Changes in the atmospheric $CH_4$ gradient between Greenland and Antarctica during the Last Glacial and the transitions to the Holocene". In: *Geophys. Res. Lett.* 27 (2000), pp. 1005–1008.

[15] Willi Dansgaard. *Frozen Annals*. Narayana Press, 2004, pp. 64–68. ISBN: 87-990078-0-0.

[16] T Güllük, H E Wagner, and F Slemr. "A high-frequency modulated tunable diode laser absorption spectrometer for measurements of $CO_2$, $CH_4$, $N_2O$, and CO in air samples of a few $cm^3$". In: *Review of Scientific Instruments* 68 (1997), pp. 230–239.

[17] C U Hammer, H B Clausen, and W Dansgaard. “Continuous impurity analysis along the Dye-3 deep core”. In: Geophysical Monograph 33. American Geophysical Union, 1985. Chap. Greenland Ice Core: Geophysics, Geochemistry, and the Environment.

[18] IPCC. *Climate Change 2013: The Physical Science Basis. Contribution of Working Group I to the Fifth Assessment Report of the Intergovernmental Panel on Climate Change [Stocker, T.F., D. Qin, G.-K. Plattner, M. Tignor, S.K. Allen, J. Boschung, A. Nauels, Y. Xia, V. Bex and P.M. Midgley (eds.)]* Cambridge University Press, Cambridge, United Kingdom and New York, NY, USA, 2013, pp. 505 –510.

[19] Patrik R. Kaufmann et al. “An Improved Continuous Flow Analysis System for High-Resolution Field Measurements on Ice Cores”. In: *Environ. Sci. Technol.* 42 (21 2008), pp. 8044 –8050.

[20] A Landais et al. “A tentative reconstruction of the last interglacial and glacial inception in Greenland based on new gas measurements in the Greenland Ice Core Project (GRIP) ice core”. In: *Journal of Geophysical Research* 108 (D18 2013), p. 4563.

[21] James E Lee et al. “Excess methane in Greenland ice cores associated with high dust concentrations”. In: *Geochimica et Cosmochimica Acta* 270 (2020), pp. 409–430.

[22] Zugang Mao and Susan B. Sinnott. “Separation of Organic Molecular Mixtures in Carbon Nanotubes and Bundles: Molecular Dynamics Simulations”. In: *J. Phys. Chem. B* 105 (2001), pp. 6916–6924.

[23] S O Rasmussen et al. “A new Greenland ice core chronology for the last glacial termination”. In: *Journal of Geophysical Research* 111 (D06102 2006).

[24] Regine Röthlisberger et al. “Technique for Continuous High-Resolution Analysis of Trace Substances in Firn and Ice Cores”. In: *Environ. Sci. Technol.* 34 (2 2000), pp. 338 –342.

[25] Urs Ruth et al. “Continuous record of microparticle concentration and size distribution in the central Greenland NGRIP ice core during the last glacial period”. In: *Journal of Geophysical Research* 108 (D3 2003), p. 4098.

[26] R Sander. “Compilation of Henry’s law constants (version 4.0) for water as solvent”. In: *Atmos. Chem. Phys.* 15 (2015), pp. 4399–4981.

[27] Simon Schüpbach et al. “A New Method for High-Resolution Methane Measurements on Polar Ice Cores Using Continuous Flow Analysis”. In: *Environ. Sci. Technol.* 43 (14 2009), pp. 5371–5376.

[28] B Stauffer et al. “Methane concentration in the glacial atmosphere was only half that of the preindustrial Holocene”. In: *Nature* 332 (1988), pp. 812–814.

[29] C Stowasser et al. “A low-volume cavity ring-down spectrometer for sample-limited applications”. In: *Appl. Phys. B* 116 (2014), pp. 255–270.

[30] C Stowasser et al. “Conituous measurements of methane mixing ratios from ice cores”. In: *Atmos. Meas. Tech.* (5 2012), pp. 999–1013.

[31] Anders Svensson, Pierre E Biscaye, and Francis E Grousset. “Characterization of late glacial continental dust in the Greenland Ice Core Project ice core”. In: *Journal of Geophysical Research* 105 (D4 2000), pp. 4637–4656.

[32] UNFCCC. *Global Warming Potentials (IPCC Second Assessment Report)*. URL: https://unfccc.int/process/transparency-and-reporting/greenhouse-gas-data/greenhouse-gas-data-unfccc/global-warming-potentials. Accessed on 03/01/2020.

[33] B Vinther, S Buchardt, and H Clausen *et al.* "Holocene thinning of the Greenland ice sheet, Supplementary Information". In: *Nature* 461 (2009), pp. 385–388.

[34] Diana Vladimirova. *High-resolution methane record of the RECAP ice core (Eastern Greenland) over the last climatic cycle*. PhD Thesis, University of Copenhagen, 2018, p. 40.

[35] Audrey M. Yau et al. "Setting a chronology for the basal ice at Dye-3 and GRIP: Implications for the long-term stability of the Greenland Ice Sheet". In: *Earth and Planetary Science Letters* 451 (2016), pp. 1–9.

# 7 Appendix I

Results from pressure and flow experiments on the micromodule.

**Figure 31:** *Measurement outputs for expected total flow 18 ml/min (Figure 32)*

| Total Flow Exp (ml/min) | Gas % | MFC (ml/min) | Pump (ml/min) | BPR (mbar) | Flg (ml/min) | σ - gas | Fl-liq (ml/min) | σ - liq | Flg/MFC | Total Flow Meas (ml/min) | Gas % Meas |
|---|---|---|---|---|---|---|---|---|---|---|---|
| **18** | 7 | 1.26 | 16.7 | 250 | 1.2534 | 0.0546 | 14.849 | 0.0772 | 0.994762 | 16.1021 | 7.784078 |
| **18** | 7 | 1.26 | 16.7 | 300 | 1.2403 | 0.0562 | 14.82 | 0.0764 | 0.984365 | 16.0604 | 7.722722 |
| **18** | 7 | 1.26 | 16.7 | 350 | 1.2266 | 0.0569 | 14.806 | 0.0962 | 0.973492 | 16.0328 | 7.650566 |
| **18** | 7 | 1.26 | 16.7 | 400 | 1.2087 | 0.0478 | 14.777 | 0.078 | 0.959286 | 15.9861 | 7.560944 |
| **18** | 7 | 1.26 | 16.7 | 450 | 1.2035 | 0.0442 | 14.749 | 0.0811 | 0.955159 | 15.9527 | 7.544177 |
| **18** | 7 | 1.26 | 16.7 | 500 | 1.1919 | 0.0484 | 14.725 | 0.0852 | 0.945952 | 15.9166 | 7.488408 |
| **18** | 9 | 1.62 | 16.4 | 250 | 1.6095 | 0.0523 | 14.589 | 0.1103 | 0.993519 | 16.1983 | 9.936228 |
| **18** | 9 | 1.62 | 16.4 | 300 | 1.5918 | 0.0449 | 14.531 | 0.1066 | 0.982593 | 16.1232 | 9.87273 |
| **18** | 9 | 1.62 | 16.4 | 350 | 1.5841 | 0.0512 | 14.52 | 0.1065 | 0.97784 | 16.1042 | 9.836564 |
| **18** | 9 | 1.62 | 16.4 | 400 | 1.5717 | 0.0423 | 14.521 | 0.0976 | 0.970185 | 16.0926 | 9.766601 |
| **18** | 9 | 1.62 | 16.4 | 450 | 1.5552 | 0.0438 | 14.533 | 0.1012 | 0.96 | 16.0879 | 9.666893 |
| **18** | 9 | 1.62 | 16.4 | 500 | 1.5488 | 0.0458 | 14.521 | 0.1132 | 0.956049 | 16.07 | 9.637834 |
| **18** | 10 | 1.8 | 16.2 | 250 | 1.7702 | 0.0485 | 14.426 | 0.1078 | 0.983444 | 16.1959 | 10.92993 |
| **18** | 10 | 1.8 | 16.2 | 300 | 1.7606 | 0.0513 | 14.427 | 0.1129 | 0.978111 | 16.1878 | 10.87609 |
| **18** | 10 | 1.8 | 16.2 | 350 | 1.7526 | 0.0493 | 14.416 | 0.1228 | 0.973667 | 16.1687 | 10.83946 |
| **18** | 10 | 1.8 | 16.2 | 400 | 1.7442 | 0.0477 | 14.445 | 0.1204 | 0.969 | 16.1891 | 10.77392 |
| **18** | 10 | 1.8 | 16.2 | 450 | 1.7257 | 0.0407 | 14.449 | 0.1097 | 0.958722 | 16.1745 | 10.66926 |
| **18** | 10 | 1.8 | 16.2 | 500 | 1.7138 | 0.0385 | 14.444 | 0.1173 | 0.952111 | 16.1575 | 10.60684 |
| **18** | 11 | 1.98 | 16 | 250 | 1.9466 | 0.0464 | 14.267 | 0.1158 | 0.983131 | 16.2139 | 12.00575 |
| **18** | 11 | 1.98 | 16 | 300 | 1.9346 | 0.0484 | 14.284 | 0.1262 | 0.977071 | 16.219 | 11.92799 |
| **18** | 11 | 1.98 | 16 | 350 | 1.9261 | 0.0483 | 14.3 | 0.1262 | 0.972778 | 16.2259 | 11.87053 |
| **18** | 11 | 1.98 | 16 | 400 | 1.9106 | 0.0426 | 14.296 | 0.1264 | 0.964949 | 16.2069 | 11.78881 |
| **18** | 11 | 1.98 | 16 | 450 | 1.905 | 0.044 | 14.291 | 0.115 | 0.962121 | 16.1957 | 11.76238 |
| **18** | 11 | 1.98 | 16 | 500 | 1.89 | 0.0385 | 14.302 | 0.1285 | 0.954545 | 16.1915 | 11.67279 |
| **18** | 13 | 2.34 | 15.7 | 250 | 2.2872 | 0.0408 | 14.031 | 0.1162 | 0.977436 | 16.3184 | 14.01608 |
| **18** | 13 | 2.34 | 15.7 | 300 | 2.2807 | 0.0466 | 14.036 | 0.1233 | 0.974658 | 16.3162 | 13.97813 |
| **18** | 13 | 2.34 | 15.7 | 350 | 2.2714 | 0.0464 | 14.03 | 0.1046 | 0.970684 | 16.3015 | 13.93369 |
| **18** | 13 | 2.34 | 15.7 | 400 | 2.2599 | 0.0437 | 14.023 | 0.1005 | 0.965769 | 16.2831 | 13.87881 |
| **18** | 13 | 2.34 | 15.7 | 450 | 2.2472 | 0.0404 | 14.023 | 0.0994 | 0.960342 | 16.2705 | 13.8115 |
| **18** | 13 | 2.34 | 15.7 | 500 | 2.2385 | 0.0432 | 14.011 | 0.1237 | 0.956624 | 16.249 | 13.77623 |
| **18** | 15 | 2.7 | 15.3 | 250 | 2.6321 | 0.0336 | 13.678 | 0.0772 | 0.974852 | 16.3105 | 16.13746 |
| **18** | 15 | 2.7 | 15.3 | 300 | 2.625 | 0.0406 | 13.679 | 0.0922 | 0.972222 | 16.3044 | 16.09995 |
| **18** | 15 | 2.7 | 15.3 | 350 | 2.615 | 0.037 | 13.689 | 0.0836 | 0.968519 | 16.3041 | 16.03891 |
| **18** | 15 | 2.7 | 15.3 | 400 | 2.6102 | 0.0457 | 13.684 | 0.0745 | 0.966741 | 16.2945 | 16.0189 |
| **18** | 15 | 2.7 | 15.3 | 450 | 2.6008 | 0.0451 | 13.699 | 0.0739 | 0.963259 | 16.3 | 15.95583 |
| **18** | 15 | 2.7 | 15.3 | 500 | 2.589 | 0.0404 | 13.708 | 0.0773 | 0.958889 | 16.2973 | 15.88607 |

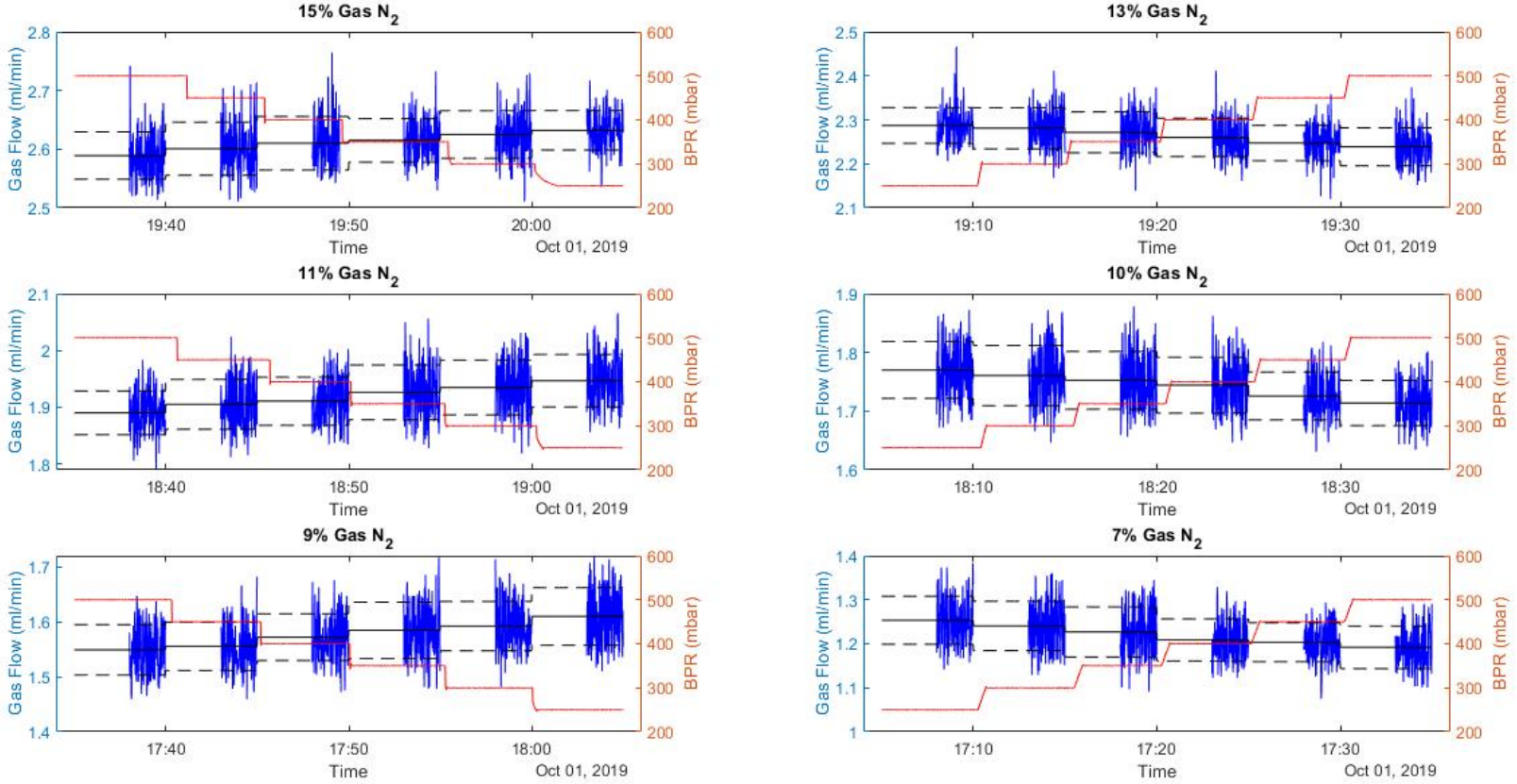


**Figure 32:** *Pressure-Flow calibration runs at various gas percentages and BPR setpoints for expected total flow 18 ml/min*

**Figure 33:** *Measurement outputs for expected total flow 20 ml/min (Figure 34)*

| Total Flow Exp (ml/min) | Gas % | MFC (ml/min) | Pump (ml/min) | BPR (mbar) | Flg (ml/min) | σ - gas | Fl-liq (ml/min) | σ - liq | Flg/MFC | Total Flow Meas (ml/min) | Gas % Meas |
|---|---|---|---|---|---|---|---|---|---|---|---|
| **20** | 7 | 1.4 | 18.6 | 250 | 1.384 | 0.0539 | 16.0114 | 0.0858 | 0.988571 | 17.3954 | 7.956126 |
| **20** | 7 | 1.4 | 18.6 | 300 | 1.366 | 0.0527 | 16.0177 | 0.0866 | 0.975714 | 17.3837 | 7.857936 |
| **20** | 7 | 1.4 | 18.6 | 350 | 1.3531 | 0.0395 | 16.0164 | 0.0846 | 0.9665 | 17.3695 | 7.790092 |
| **20** | 7 | 1.4 | 18.6 | 400 | 1.3413 | 0.044 | 16.0069 | 0.083 | 0.958071 | 17.3482 | 7.731638 |
| **20** | 7 | 1.4 | 18.6 | 450 | 1.3217 | 0.043 | 16.0174 | 0.0873 | 0.944071 | 17.3391 | 7.622656 |
| **20** | 7 | 1.4 | 18.6 | 500 | 1.3093 | 0.0418 | 16.0132 | 0.0816 | 0.935214 | 17.3225 | 7.558378 |
| **20** | 9 | 1.8 | 18.2 | 250 | 1.7703 | 0.0454 | 15.6971 | 0.1039 | 0.9835 | 17.4674 | 10.13488 |
| **20** | 9 | 1.8 | 18.2 | 300 | 1.7593 | 0.0437 | 15.7006 | 0.0935 | 0.977389 | 17.4599 | 10.07623 |
| **20** | 9 | 1.8 | 18.2 | 350 | 1.7477 | 0.0414 | 15.7088 | 0.09 | 0.970944 | 17.4565 | 10.01174 |
| **20** | 9 | 1.8 | 18.2 | 400 | 1.7252 | 0.0393 | 15.7055 | 0.1027 | 0.958444 | 17.4307 | 9.89748 |
| **20** | 9 | 1.8 | 18.2 | 450 | 1.7151 | 0.0391 | 15.7063 | 0.1017 | 0.952833 | 17.4214 | 9.844789 |
| **20** | 9 | 1.8 | 18.2 | 500 | 1.6995 | 0.0353 | 15.7227 | 0.1017 | 0.944167 | 17.4222 | 9.754796 |
| **20** | 10 | 2 | 18 | 250 | 1.9586 | 0.0444 | 15.5539 | 0.1158 | 0.9793 | 17.5125 | 11.18401 |
| **20** | 10 | 2 | 18 | 300 | 1.9503 | 0.0463 | 15.5315 | 0.116 | 0.97515 | 17.4818 | 11.15617 |
| **20** | 10 | 2 | 18 | 350 | 1.9275 | 0.0433 | 15.5472 | 0.1355 | 0.96375 | 17.4747 | 11.03023 |
| **20** | 10 | 2 | 18 | 400 | 1.9179 | 0.0386 | 15.5387 | 0.1025 | 0.95895 | 17.4566 | 10.98668 |
| **20** | 10 | 2 | 18 | 450 | 1.9013 | 0.0393 | 15.5407 | 0.1073 | 0.95065 | 17.442 | 10.9007 |
| **20** | 10 | 2 | 18 | 500 | 1.8949 | 0.0423 | 15.5139 | 0.1108 | 0.94745 | 17.4088 | 10.88472 |
| **20** | 11 | 2.2 | 17.8 | 250 | 2.1531 | 0.0447 | 15.3491 | 0.0917 | 0.978682 | 17.5022 | 12.30188 |
| **20** | 11 | 2.2 | 17.8 | 300 | 2.1388 | 0.0452 | 15.3655 | 0.0984 | 0.972182 | 17.5043 | 12.21871 |
| **20** | 11 | 2.2 | 17.8 | 350 | 2.1281 | 0.0408 | 15.3749 | 0.1018 | 0.967318 | 17.503 | 12.15849 |
| **20** | 11 | 2.2 | 17.8 | 400 | 2.1128 | 0.0406 | 15.3863 | 0.0919 | 0.960364 | 17.4991 | 12.07376 |
| **20** | 11 | 2.2 | 17.8 | 450 | 2.1043 | 0.0378 | 15.3831 | 0.0928 | 0.9565 | 17.4874 | 12.03324 |
| **20** | 11 | 2.2 | 17.8 | 500 | 2.0902 | 0.0418 | 15.3774 | 0.1106 | 0.950091 | 17.4676 | 11.96615 |
| **20** | 13 | 2.6 | 17.4 | 250 | 2.5269 | 0.0349 | 15.0808 | 0.0678 | 0.971885 | 17.6077 | 14.35111 |
| **20** | 13 | 2.6 | 17.4 | 300 | 2.515 | 0.0424 | 15.0834 | 0.0692 | 0.967308 | 17.5984 | 14.29107 |
| **20** | 13 | 2.6 | 17.4 | 350 | 2.4998 | 0.0414 | 15.0793 | 0.0657 | 0.961462 | 17.5791 | 14.2203 |
| **20** | 13 | 2.6 | 17.4 | 400 | 2.4944 | 0.0383 | 15.0532 | 0.0674 | 0.959385 | 17.5476 | 14.21505 |
| **20** | 13 | 2.6 | 17.4 | 450 | 2.4848 | 0.0341 | 15.0419 | 0.0686 | 0.955692 | 17.5267 | 14.17723 |
| **20** | 13 | 2.6 | 17.4 | 500 | 2.4781 | 0.0417 | 15.0449 | 0.0705 | 0.953115 | 17.523 | 14.14198 |
| **20** | 15 | 3 | 17 | 250 | 2.9132 | 0.0127 | 14.7509 | 0.0626 | 0.971067 | 17.6641 | 16.49221 |
| **20** | 15 | 3 | 17 | 300 | 2.8996 | 0.0362 | 14.7563 | 0.0668 | 0.966533 | 17.6559 | 16.42284 |
| **20** | 15 | 3 | 17 | 350 | 2.8952 | 0.0498 | 14.7388 | 0.0706 | 0.965067 | 17.634 | 16.41828 |
| **20** | 15 | 3 | 17 | 400 | 2.8843 | 0.0564 | 14.7562 | 0.0715 | 0.961433 | 17.6405 | 16.35044 |
| **20** | 15 | 3 | 17 | 450 | 2.876 | 0.048 | 14.7531 | 0.0663 | 0.958667 | 17.6291 | 16.31394 |
| **20** | 15 | 3 | 17 | 500 | 2.8605 | 0.0413 | 14.7682 | 0.0726 | 0.9535 | 17.6287 | 16.22638 |

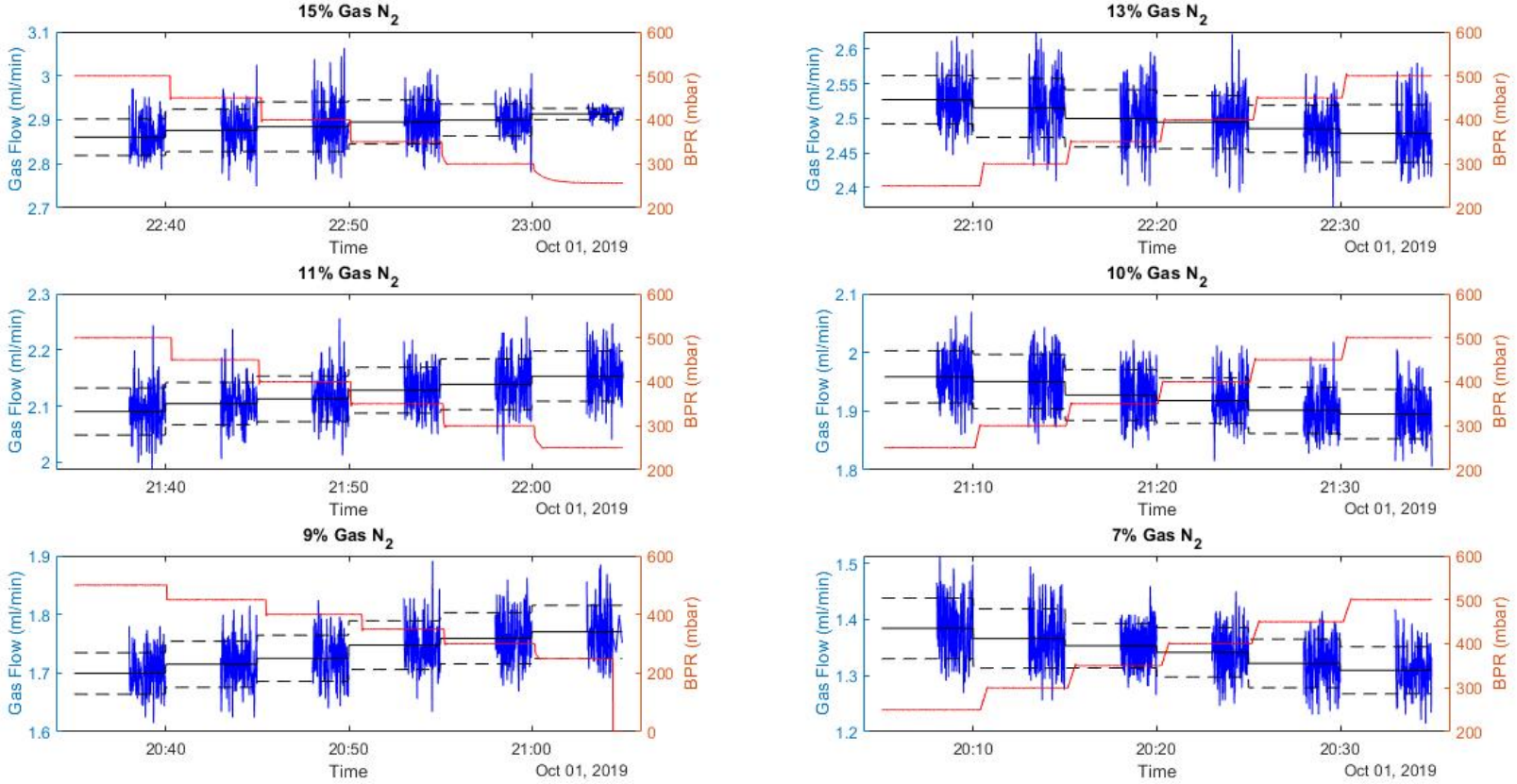


**Figure 34:** *Pressure-Flow calibration runs at various gas percentages and BPR setpoints for expected total flow 20 ml/min*

**Figure 35:** *Measurement outputs for expected total flow 23 ml/min (Figure 36)*

| Total Flow Exp (ml/min) | Gas % | MFC (ml/min) | Pump (ml/min) | BPR (mbar) | Flg (ml/min) | σ - gas | Fl-liq (ml/min) | σ - liq | Flg/MFC | Total Flow Meas (ml/min) | Gas % Meas |
|---|---|---|---|---|---|---|---|---|---|---|---|
| **23** | 7 | 1.61 | 21.4 | 250 | 1.5737 | 0.04 | 17.4214 | 0.3938 | 0.977453 | 18.9951 | 8.284768 |
| **23** | 7 | 1.61 | 21.4 | 300 | 1.5655 | 0.047 | 17.4534 | 0.388 | 0.97236 | 19.0189 | 8.231286 |
| **23** | 7 | 1.61 | 21.4 | 350 | 1.5461 | 0.039 | 17.4738 | 0.3916 | 0.960311 | 19.0199 | 8.128855 |
| **23** | 7 | 1.61 | 21.4 | 400 | 1.5316 | 0.047 | 17.4959 | 0.3941 | 0.951304 | 19.0275 | 8.049402 |
| **23** | 7 | 1.61 | 21.4 | 450 | 1.5166 | 0.049 | 17.5213 | 0.3999 | 0.941988 | 19.0379 | 7.966215 |
| **23** | 7 | 1.61 | 21.4 | 500 | 1.4961 | 0.04 | 17.5073 | 0.404 | 0.929255 | 19.0034 | 7.872802 |
| **23** | 9 | 2.07 | 20.9 | 250 | 2.0189 | 0.042 | 17.3515 | 0.4271 | 0.975314 | 19.3704 | 10.4226 |
| **23** | 9 | 2.07 | 20.9 | 300 | 2.0055 | 0.041 | 17.2979 | 0.4217 | 0.968841 | 19.3034 | 10.38936 |
| **23** | 9 | 2.07 | 20.9 | 350 | 1.9888 | 0.042 | 17.2509 | 0.4233 | 0.960773 | 19.2397 | 10.33696 |
| **23** | 9 | 2.07 | 20.9 | 400 | 1.9738 | 0.043 | 17.2615 | 0.4355 | 0.953527 | 19.2353 | 10.26134 |
| **23** | 9 | 2.07 | 20.9 | 450 | 1.9627 | 0.048 | 17.2395 | 0.4237 | 0.948164 | 19.2022 | 10.22122 |
| **23** | 9 | 2.07 | 20.9 | 500 | 1.9442 | 0.046 | 17.1997 | 0.4232 | 0.939227 | 19.1439 | 10.15572 |
| **23** | 10 | 2.3 | 20.7 | 250 | 2.2408 | 0.046 | 17.2401 | 0.4222 | 0.974261 | 19.4809 | 11.50255 |
| **23** | 10 | 2.3 | 20.7 | 300 | 2.2316 | 0.051 | 17.2427 | 0.4273 | 0.970261 | 19.4743 | 11.45921 |
| **23** | 10 | 2.3 | 20.7 | 350 | 2.2121 | 0.053 | 17.2659 | 0.4218 | 0.961783 | 19.478 | 11.35692 |
| **23** | 10 | 2.3 | 20.7 | 400 | 2.1978 | 0.045 | 17.2782 | 0.4196 | 0.955565 | 19.476 | 11.28466 |
| **23** | 10 | 2.3 | 20.7 | 450 | 2.1875 | 0.05 | 17.3012 | 0.4162 | 0.951087 | 19.4887 | 11.22445 |
| **23** | 10 | 2.3 | 20.7 | 500 | 2.167 | 0.045 | 17.2876 | 0.4192 | 0.942174 | 19.4546 | 11.13875 |
| **23** | 11 | 2.53 | 20.5 | 250 | 2.4588 | 0.043 | 17.2572 | 0.4167 | 0.971858 | 19.716 | 12.47109 |
| **23** | 11 | 2.53 | 20.5 | 300 | 2.4442 | 0.053 | 17.2598 | 0.3924 | 0.966087 | 19.704 | 12.40459 |
| **23** | 11 | 2.53 | 20.5 | 350 | 2.4314 | 0.056 | 17.2423 | 0.3915 | 0.961028 | 19.6737 | 12.35863 |
| **23** | 11 | 2.53 | 20.5 | 400 | 2.4142 | 0.065 | 17.2226 | 0.3967 | 0.954229 | 19.6368 | 12.29426 |
| **23** | 11 | 2.53 | 20.5 | 450 | 2.4037 | 0.053 | 17.189 | 0.3937 | 0.950079 | 19.5927 | 12.26834 |
| **23** | 11 | 2.53 | 20.5 | 500 | 2.3914 | 0.062 | 17.1738 | 0.3894 | 0.945217 | 19.5652 | 12.22272 |
| **23** | 13 | 2.99 | 20 | 250 | 2.9003 | 0.015 | 16.9302 | 0.297 | 0.97 | 19.8305 | 14.62545 |
| **23** | 13 | 2.99 | 20 | 300 | 2.8875 | 0.068 | 16.9325 | 0.2973 | 0.965719 | 19.82 | 14.56862 |
| **23** | 13 | 2.99 | 20 | 350 | 2.8803 | 0.069 | 16.9377 | 0.297 | 0.963311 | 19.818 | 14.53376 |
| **23** | 13 | 2.99 | 20 | 400 | 2.8602 | 0.061 | 16.9286 | 0.2916 | 0.956589 | 19.7888 | 14.45363 |
| **23** | 13 | 2.99 | 20 | 450 | 2.8483 | 0.058 | 16.9518 | 0.297 | 0.952609 | 19.8001 | 14.38528 |
| **23** | 13 | 2.99 | 20 | 500 | 2.8419 | 0.062 | 16.9627 | 0.3035 | 0.950468 | 19.8046 | 14.3497 |
| **23** | 15 | 3.45 | 19.6 | 250 | 3.3444 | 0.013 | 16.7908 | 0.2025 | 0.969391 | 20.1352 | 16.60972 |
| **23** | 15 | 3.45 | 19.6 | 300 | 3.3386 | 0.06 | 16.7702 | 0.1962 | 0.96771 | 20.1088 | 16.60268 |
| **23** | 15 | 3.45 | 19.6 | 350 | 3.319 | 0.064 | 16.7473 | 0.1946 | 0.962029 | 20.0663 | 16.54017 |
| **23** | 15 | 3.45 | 19.6 | 400 | 3.3118 | 0.057 | 16.7386 | 0.1982 | 0.959942 | 20.0504 | 16.51738 |
| **23** | 15 | 3.45 | 19.6 | 450 | 3.299 | 0.056 | 16.752 | 0.1952 | 0.956232 | 20.051 | 16.45304 |
| **23** | 15 | 3.45 | 19.6 | 500 | 3.2906 | 0.07 | 16.7333 | 0.1955 | 0.953797 | 20.0239 | 16.43336 |

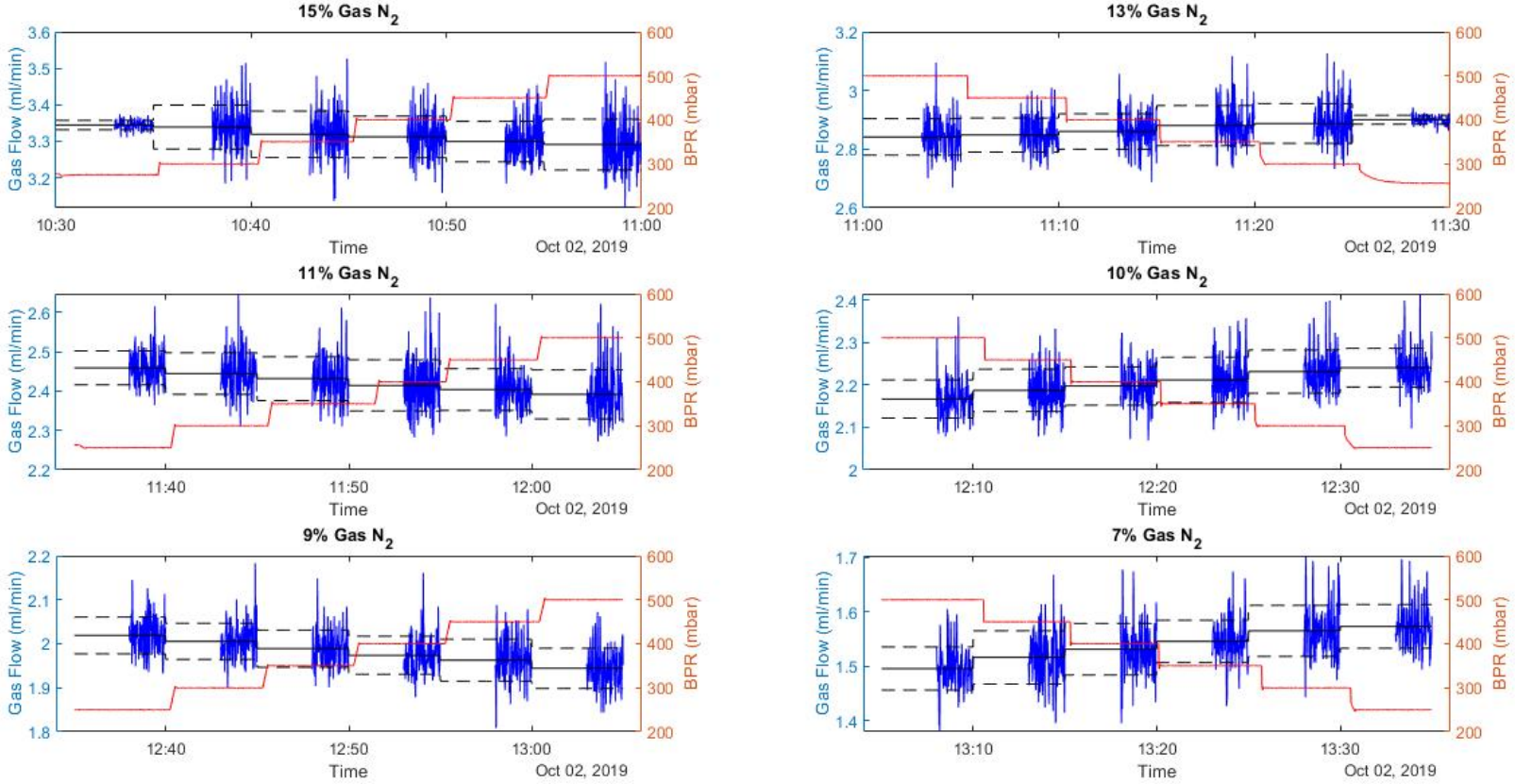


**Figure 36:** *Pressure-Flow calibration runs at various gas percentages and BPR setpoints for expected total flow 23 ml/min*

**Figure 37:** *Measurement outputs for expected total flow 25 ml/min (Figure 38). NOTE: Data for 450 mbar BPR setpoint for this run was lost.*

| Total Flow Exp (ml/min) | Gas % | MFC (ml/min) | Pump (ml/min) | BPR (mbar) | FIg (ml/min) | σ - gas | FI-liq (ml/min) | σ - liq | FIg/MFC | Total Flow Meas (ml/min) | Gas % Meas |
|---|---|---|---|---|---|---|---|---|---|---|---|
| **25** | 7 | 1.75 | 23.3 | 250 | 1.7085 | 0.0419 | 19.0043 | 0.1093 | 0.976286 | 20.7128 | 8.248523 |
| **25** | 7 | 1.75 | 23.3 | 300 | 1.6878 | 0.0414 | 19.0184 | 0.102 | 0.964457 | 20.7062 | 8.151182 |
| **25** | 7 | 1.75 | 23.3 | 350 | 1.6686 | 0.0377 | 19.04 | 0.1036 | 0.953486 | 20.7086 | 8.057522 |
| **25** | 7 | 1.75 | 23.3 | 400 | 1.6555 | 0.0415 | 19.0541 | 0.1041 | 0.946 | 20.7096 | 7.993877 |
| **25** | 7 | 1.75 | 23.3 | 450 | NaN | NaN | NaN | NaN | NaN | NaN | NaN |
| **25** | 7 | 1.75 | 23.3 | 500 | 1.6128 | 0.0332 | 19.0703 | 0.1025 | 0.9216 | 20.6831 | 7.797671 |
| **25** | 9 | 2.25 | 22.8 | 250 | 2.1825 | 0.0411 | 18.8509 | 0.1057 | 0.97 | 21.0334 | 10.37635 |
| **25** | 9 | 2.25 | 22.8 | 300 | 2.1621 | 0.038 | 18.8383 | 0.1167 | 0.960933 | 21.0004 | 10.29552 |
| **25** | 9 | 2.25 | 22.8 | 350 | 2.1452 | 0.0314 | 18.8321 | 0.1167 | 0.953422 | 20.9773 | 10.22629 |
| **25** | 9 | 2.25 | 22.8 | 400 | 2.1295 | 0.0327 | 18.8422 | 0.1052 | 0.946444 | 20.9717 | 10.15416 |
| **25** | 9 | 2.25 | 22.8 | 450 | 2.1118 | 0.0325 | 18.8338 | 0.1145 | 0.938578 | 20.9456 | 10.08231 |
| **25** | 9 | 2.25 | 22.8 | 500 | 2.0958 | 0.0365 | 18.7877 | 0.1105 | 0.931467 | 20.8835 | 10.03567 |
| **25** | 10 | 2.5 | 22.5 | 250 | 2.3466 | 0.0381 | 18.7436 | 0.1578 | 0.93864 | 21.0902 | 11.12649 |
| **25** | 10 | 2.5 | 22.5 | 300 | 2.3611 | 0.0367 | 18.7063 | 0.1573 | 0.94444 | 21.0674 | 11.20736 |
| **25** | 10 | 2.5 | 22.5 | 350 | 2.3739 | 0.0433 | 18.7122 | 0.1586 | 0.94956 | 21.0861 | 11.25813 |
| **25** | 10 | 2.5 | 22.5 | 400 | 2.3902 | 0.0399 | 18.7027 | 0.1604 | 0.95608 | 21.0929 | 11.33178 |
| **25** | 10 | 2.5 | 22.5 | 450 | 2.4053 | 0.0371 | 18.6909 | 0.1576 | 0.96212 | 21.0962 | 11.40158 |
| **25** | 10 | 2.5 | 22.5 | 500 | 2.4131 | 0.0372 | 18.6767 | 0.1675 | 0.96524 | 21.0898 | 11.44202 |
| **25** | 11 | 2.75 | 22.3 | 250 | 2.6563 | 0.0335 | 18.6574 | 0.2052 | 0.965927 | 21.3137 | 12.46288 |
| **25** | 11 | 2.75 | 22.3 | 300 | 2.6424 | 0.0381 | 18.6394 | 0.197 | 0.960873 | 21.2818 | 12.41624 |
| **25** | 11 | 2.75 | 22.3 | 350 | 2.6271 | 0.0346 | 18.625 | 0.1948 | 0.955309 | 21.2521 | 12.3616 |
| **25** | 11 | 2.75 | 22.3 | 400 | 2.6133 | 0.0402 | 18.6313 | 0.1915 | 0.950291 | 21.2446 | 12.30101 |
| **25** | 11 | 2.75 | 22.3 | 450 | 2.5947 | 0.0469 | 18.6552 | 0.1948 | 0.943527 | 21.2499 | 12.21041 |
| **25** | 11 | 2.75 | 22.3 | 500 | 2.5818 | 0.041 | 18.6698 | 0.2052 | 0.938836 | 21.2516 | 12.14873 |
| **25** | 13 | 3.25 | 21.8 | 250 | 3.1386 | 0.0147 | 18.3664 | 0.3215 | 0.965723 | 21.505 | 14.59475 |
| **25** | 13 | 3.25 | 21.8 | 300 | 3.1282 | 0.0421 | 18.3753 | 0.3169 | 0.962523 | 21.5035 | 14.5474 |
| **25** | 13 | 3.25 | 21.8 | 350 | 3.1179 | 0.0478 | 18.3628 | 0.3122 | 0.959354 | 21.4807 | 14.51489 |
| **25** | 13 | 3.25 | 21.8 | 400 | 3.1036 | 0.0448 | 18.3756 | 0.3038 | 0.954954 | 21.4792 | 14.44933 |
| **25** | 13 | 3.25 | 21.8 | 450 | 3.0888 | 0.0478 | 18.3861 | 0.3038 | 0.9504 | 21.4749 | 14.3833 |
| **25** | 13 | 3.25 | 21.8 | 500 | 3.0709 | 0.0391 | 18.4013 | 0.2885 | 0.944892 | 21.4722 | 14.30175 |
| **25** | 15 | 3.75 | 21.3 | 250 | 3.6354 | 0.0142 | 18.0207 | 0.2793 | 0.96944 | 21.6561 | 16.78696 |
| **25** | 15 | 3.75 | 21.3 | 300 | 3.6199 | 0.0346 | 18.123 | 0.2965 | 0.965307 | 21.7429 | 16.64865 |
| **25** | 15 | 3.75 | 21.3 | 350 | 3.6024 | 0.0435 | 18.0898 | 0.3201 | 0.96064 | 21.6922 | 16.60689 |
| **25** | 15 | 3.75 | 21.3 | 400 | 3.5964 | 0.0486 | 18.0875 | 0.3413 | 0.95904 | 21.6839 | 16.58558 |
| **25** | 15 | 3.75 | 21.3 | 450 | 3.5717 | 0.0521 | 18.062 | 0.3398 | 0.952453 | 21.6337 | 16.50989 |
| **25** | 15 | 3.75 | 21.3 | 500 | 3.562 | 0.0538 | 18.093 | 0.3663 | 0.949867 | 21.655 | 16.44886 |

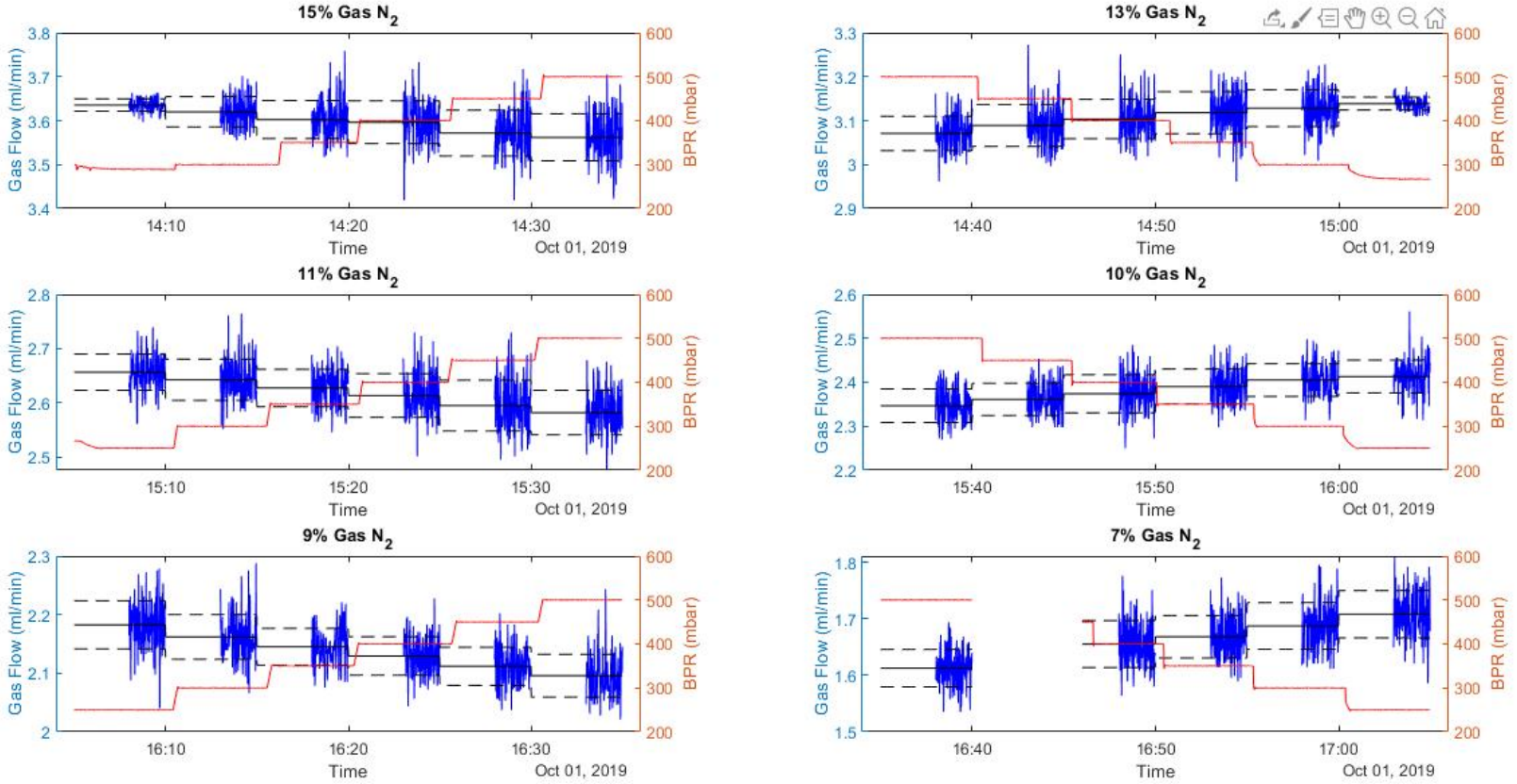


**Figure 38:** *Pressure-Flow calibration runs at various gas percentages and BPR setpoints for expected total flow 25 ml/min. NOTE: Data for 450 mbar BPR setpoint for this run was lost.*

# 8 Appendix II

Offset of bag lengths calculated from encoder, from actual measured lengths in the CFA freezer taken as (Freezer - Calculated). Negative offset values indicate longer lengths calculated from encoder and positive values indicate shorter. Yellow highlighted values are bags with an offset greater than 1 cm. Horizontal row lines mark the bags in each measurement run. Blue highlighted values show the sum offset of all the bags in one run, while the orange highlighted cell is the total offset for all the bags measured during the campaign.

| BagNo | baglength Freezer (cm) | bagoffset (m) | Sum Offset run (m) | Total Offset (m) |
|---|---|---|---|---|
| 1704 | 102.3 | -0.002 | | -0.0564 |
| 1705 | 102.1 | -0.004 | | |
| 1706 | 98.2 | 0.008 | | |
| 1707 | 101.4 | 0.007 | | |
| 1708 | 100.2 | 0.001 | | |
| 1709 | 101.6 | -0.007 | | |
| 1710 | 100.7 | 0.012 | | |
| 1711 | 100.3 | 0.008 | 0.0223 | |
| 1712 | 99.5 | 0.003 | | |
| 1713 | 101.3 | 0.002 | | |
| 1714 | 100.5 | 0.001 | | |
| 1715 | 99.5 | 0.007 | | |
| 1716 | 100.7 | 0.008 | | |
| 1717 | 99.5 | -0.006 | | |
| 1718 | 99.5 | -0.008 | | |
| 1719 | 100 | -0.003 | 0.0046 | |
| 1720 | 99.3 | 0.001 | | |
| 1721 | 100.7 | -0.002 | | |
| 1722 | 94.3 | -0.004 | | |
| 1723 | 100.5 | -0.002 | | |
| 1724 | 101 | -0.002 | | |
| 1725 | 100.5 | -0.001 | | |
| 1726 | 101 | -0.002 | | |
| 1727 | 100.5 | -0.003 | | |
| 1728 | 101.2 | 0.020 | | |
| 1729 | 99.4 | 0.002 | 0.0066 | |
| 1730 | 103.3 | 0.005 | | |
| 1731 | 99.7 | -0.006 | | |
| 1732 | 100.7 | 0.001 | | |
| 1733 | 100.6 | -0.006 | | |
| 1734 | 99.4 | 0.008 | | |
| 1735 | 100 | 0.001 | | |
| 1736 | 101 | -0.004 | | |
| 1737 | 101.1 | -0.003 | -0.0037 | |
| 1738 | 101.5 | 0.000 | | |
| 1739 | 100.2 | -0.011 | | |
| 1740 | 101.7 | -0.002 | | |
| 1741 | 101.5 | -0.001 | | |
| 1742 | 99.7 | -0.004 | | |
| 1744 | 97.7 | -0.002 | | |
| 1746 | 100.8 | -0.004 | | |
| 1748 | 103.6 | 0.002 | | |
| 1750 | 109.5 | 0.000 | -0.0230 | |
| 1752 | 101 | -0.003 | | |
| 1754 | 100 | 0.003 | | |

| | | | |
|---|---|---|---|
| 1756 | 93.5 | 0.001 | |
| 1758 | 103 | 0.001 | |
| 1760 | 99.5 | 0.006 | |
| 1761 | 102 | 0.003 | |
| 1762 | 102.3 | -0.002 | |
| 1765 | 97.5 | 0.003 | |
| 1766 | 98 | -0.004 | |
| 1767 | 99 | -0.003 | |
| 1768 | 100.5 | -0.006 | |
| 1770 | 101 | -0.001 | -0.0022 |
| 1816 | 93.3 | -0.007 | |
| 1817 | 99.7 | -0.001 | |
| 1818 | 93.3 | -0.004 | |
| 1819 | 100 | -0.001 | |
| 1820 | 101 | -0.008 | |
| 1821 | 86 | -0.005 | |
| 1822 | 100 | 0.007 | |
| 1823 | 92.5 | -0.004 | |
| 1824 | 101.5 | 0.009 | -0.0128 |
| 1825 | 95 | 0.001 | |
| 1826 | 94.6 | 0.000 | |
| 1827 | 95.6 | -0.001 | -0.0004 |
| 1828 | 101 | 0.000 | |
| 1829 | 102.6 | 0.000 | |
| 1830 | 101.4 | 0.000 | -0.0005 |
| 1831 | 92.7 | 0.004 | |
| 1832 | 97 | -0.015 | |
| 1833 | 96.3 | -0.005 | -0.0151 |
| 1834 | 100.2 | 0.005 | |
| 1835 | 101.4 | -0.002 | |
| 1836 | 98.6 | 0.002 | |
| 1837 | 99.4 | -0.001 | |
| 1838 | 103.4 | 0.004 | |
| 1839 | 101.9 | -0.002 | |
| 1840 | 40.7 | -0.002 | |
| 1841 | 99.7 | -0.016 | |
| 1842 | 100.6 | -0.007 | -0.0191 |
| 1843 | 102.5 | 0.000 | |
| 1844 | 100 | -0.003 | |
| 1845 | 90.5 | -0.007 | |
| 1846 | 100 | 0.000 | |
| 1847 | 101 | -0.002 | |
| 1848 | 92 | -0.003 | |
| 1849 | 100 | -0.006 | |
| 1850 | 87.5 | -0.001 | |
| 1851 | 99.5 | -0.005 | |
| 1852 | 104 | 0.003 | -0.0232 |

| | | | |
|---|---|---|---|
| 1853 | 100 | 0.007 | |
| 1854 | 101.5 | -0.002 | |
| 1855 | 101.7 | 0.000 | |
| 1856 | 102 | 0.000 | |
| 1857 | 99 | -0.001 | |
| 1858 | 93 | -0.001 | |
| 1859 | 98.7 | 0.001 | |
| 1860 | 101.8 | -0.003 | |
| 1861 | 102 | 0.000 | 0.0024 |
| 1862 | 100.9 | 0.010 | |
| 1863 | 101.4 | -0.001 | |
| 1864 | 101.3 | -0.003 | 0.0061 |
| 1865 | 100.3 | 0.005 | |
| 1866 | 102.7 | 0.001 | |
| 1867 | 100.7 | -0.002 | |
| 1868 | 102.2 | -0.003 | 0.0016 |

# 9 Appendix III

Internal volume estimation between MicroModule and the Picarro

**VOLUME FROM MICROMODULE TO PICARRO**

| Flow (ml/min) | Pressure (mbar) | Switch Time | P_spike Time | CH4 Time | Δswitch-p_spike (min) | ΔP_spike-CH4 (min) | Calculated volume (ml) |
|---|---|---|---|---|---|---|---|
| 1.51 | 212.60 | 16:10:01 | 16:10:31 | 16:12:00 | 0.50 | 1.49 | 10.68 |
| 1.51 | 212.29 | 16:25:00 | 16:25:32 | 16:27:00 | 0.53 | 1.47 | 10.59 |
| 1.50 | 212.75 | 16:45:01 | 16:45:32 | 16:47:07 | 0.51 | 1.59 | 11.35 |
| 1.41 | 207.02 | 17:00:01 | 17:00:32 | 17:01:59 | 0.52 | 1.46 | 10.06 |
| 1.41 | 206.69 | 17:15:01 | 17:15:33 | 17:17:09 | 0.53 | 1.61 | 11.13 |
| 1.41 | 206.66 | 17:30:03 | 17:30:33 | 17:32:16 | 0.51 | 1.71 | 11.84 |
| 1.32 | 200.23 | 17:45:01 | 17:45:33 | 17:47:02 | 0.53 | 1.49 | 9.93 |
| 1.31 | 199.73 | 18:00:01 | 18:00:35 | 18:02:09 | 0.57 | 1.56 | 10.41 |
| 1.31 | 200.61 | 18:15:01 | 18:15:33 | 18:17:06 | 0.53 | 1.55 | 10.29 |
| 1.21 | 193.42 | 18:30:00 | 18:30:31 | 18:32:14 | 0.52 | 1.71 | 10.88 |
| 1.22 | 192.80 | 18:45:35 | 18:46:05 | 18:47:46 | 0.51 | 1.68 | 10.78 |
| 1.21 | 193.05 | 19:00:01 | 19:00:34 | 19:02:26 | 0.54 | 1.88 | 11.95 |
| 1.12 | 186.26 | 19:15:01 | 19:15:31 | 19:17:25 | 0.51 | 1.89 | 11.53 |
| 1.11 | 185.77 | 19:30:01 | 19:30:33 | 19:32:15 | 0.53 | 1.70 | 10.31 |
| 1.12 | 186.15 | 19:45:01 | 19:45:35 | 19:47:13 | 0.56 | 1.63 | 9.92 |
| 1.02 | 179.74 | 20:00:02 | 20:00:33 | 20:02:35 | 0.52 | 2.03 | 11.67 |
| 1.02 | 178.67 | 20:15:09 | 20:15:40 | 20:17:34 | 0.51 | 1.90 | 11.01 |
| 1.02 | 179.12 | 20:30:01 | 20:30:34 | 20:32:40 | 0.55 | 2.10 | 12.15 |
| 0.92 | 171.17 | 20:45:04 | 20:45:36 | 20:47:41 | 0.53 | 2.08 | 11.31 |
| 0.92 | 171.15 | 21:00:01 | 21:00:34 | 21:02:34 | 0.55 | 2.00 | 10.87 |